



TECHNICKÁ UNIVERZITA V LIBERCI
www.tul.cz



LIBEREC | ZITTAU/GÖRLITZ | JELENIA GÓRA

ACC JOURNAL XXVIII 1/2022

Issue A

Natural Sciences and Technology



IHI

Internationales
Hochschulinstitut
ZITTAU
der TU Dresden



Uniwersytet Ekonomiczny
we Wrocławiu

TECHNICKÁ UNIVERZITA V LIBERCI

HOCHSCHULE ZITTAU/GÖRLITZ

INTERNATIONALES HOCHSCHULINSTITUT ZITTAU DER TU DRESDEN

UNIwersYTET EKONOMICZNY WE WROCLAWIU

WYDZIAŁ EKONOMII, ZARZĄDZANIA I TURYSTYKI W JELENIEJ GÓRZE

Indexed in:

INDEX  COPERNICUS
I N T E R N A T I O N A L

Liberec – Zittau/Görlitz – Wrocław/Jelenia Góra

© **Technická univerzita v Liberci 2022**

ISSN 1803-9782 (Print)

ISSN 2571-0613 (Online)

ACC JOURNAL je mezinárodní vědecký časopis, jehož vydavatelem je Technická univerzita v Liberci. Na jeho tvorbě se podílí čtyři vysoké školy sdružené v Akademickém koordinačním středisku v Euroregionu Nisa (ACC). Ročně vycházejí zpravidla tři čísla.

ACC JOURNAL je periodikum publikující původní recenzované vědecké práce, vědecké studie, příspěvky ke konferencím a výzkumným projektům. První číslo obsahuje příspěvky zaměřené na oblast přírodních věd a techniky, druhé číslo je zaměřeno na oblast ekonomie, třetí číslo pojednává o tématech ze společenských věd. ACC JOURNAL má charakter recenzovaného časopisu. Jeho vydání navazuje na sborník „Vědecká pojednání“, který vycházel v letech 1995-2008.

ACC JOURNAL is an international scientific journal. It is published by the Technical University of Liberec. Four universities united in the Academic Coordination Centre in the Euroregion Nisa participate in its production. There are usually three issues of the journal annually.

ACC JOURNAL is a periodical publishing original reviewed scientific papers, scientific studies, papers presented at conferences, and findings of research projects. The first issue focuses on natural sciences and technology, the second issue deals with the science of economics, and the third issue contains findings from the area of social sciences. ACC JOURNAL is a reviewed one. It is building upon the tradition of the “Scientific Treatises” published between 1995 and 2008.

Hlavní recenzenti (major reviewers):

doc. Ing. Michal Petrů, Ph.D.

Technical University of Liberec
Faculty of Mechanical Engineering
Czech Republic

Ing. Pavel Klouček, Ph.D.

VÚTS, a.s.
Measurement Department
Czech Republic

Contents

Research Articles

Gearbox Test Rig for SkySpotter 150 Helicopter	7
Ing. Jan Bělík	
Screw Sorting Application with 6 DoF UR5e Robot Arm	14
Hamid Castillo Martinez; Emiliano Lara Romero; Ricardo Ugalde Tinoco; Ing. Christian Vogel	
Modeling of the Temporal Behavior of the Surface Temperature of an Isolation Material Test Sample under an AC Low Current Arc	30
Dipl.-Ing. (FH) Daniel Fiß; Dipl.-Ing. (FH) Stefan Kühnel; Ernest Krzyszkowski; prof. Dr. techn. Stefan Kornhuber	
Innovation of Electronic Control of the Air for the Fireplace Stove	46
Ing. Josef Hykl, MBA	
List of Authors	56
Guidelines for Contributors	57
Editorial Board	58

Research Articles

GEARBOX TEST RIG FOR SKYSPOTTER 150 HELICOPTER

Jan Bělík

VÚTS, a.s., Measurement Department,
Svárovská 619, 460 01, Liberec XI – Růžodol I, Czech Republic
e-mail: jan.belik@vuts.cz

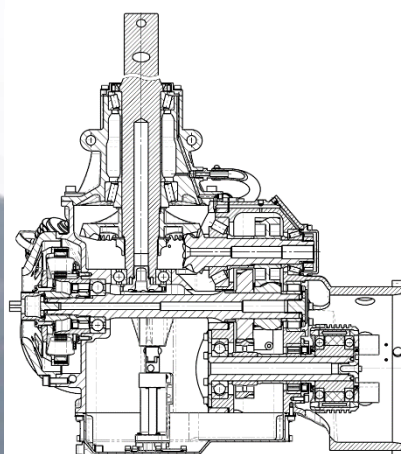
Abstract

SkySpotter 150 is an unmanned helicopter introduced recently by Modelárna LIAZ. The gearbox test rig developed for this helicopter has an innovative design. The drive is combined with a dynamometer and an axial force mechanism, which simulates the load from the main rotor on the gearbox output shaft. It leads to a special solution. The measurement methodology was developed including all sensors and design of the rig with a non-traditionally oriented dynamometer. The design has safety features that protect the test rig components and operator. The test rig is used for many tests during the development and improvement of the new helicopter generation. It also serves for verifying the gearbox parameters during its lifetime; it means tests of new gearboxes as well as technical diagnostic during periodical inspections.

Keywords

Angular gearbox; Test rig; Vibrations; Measurement.

Introduction



Source: [1] and its gearbox

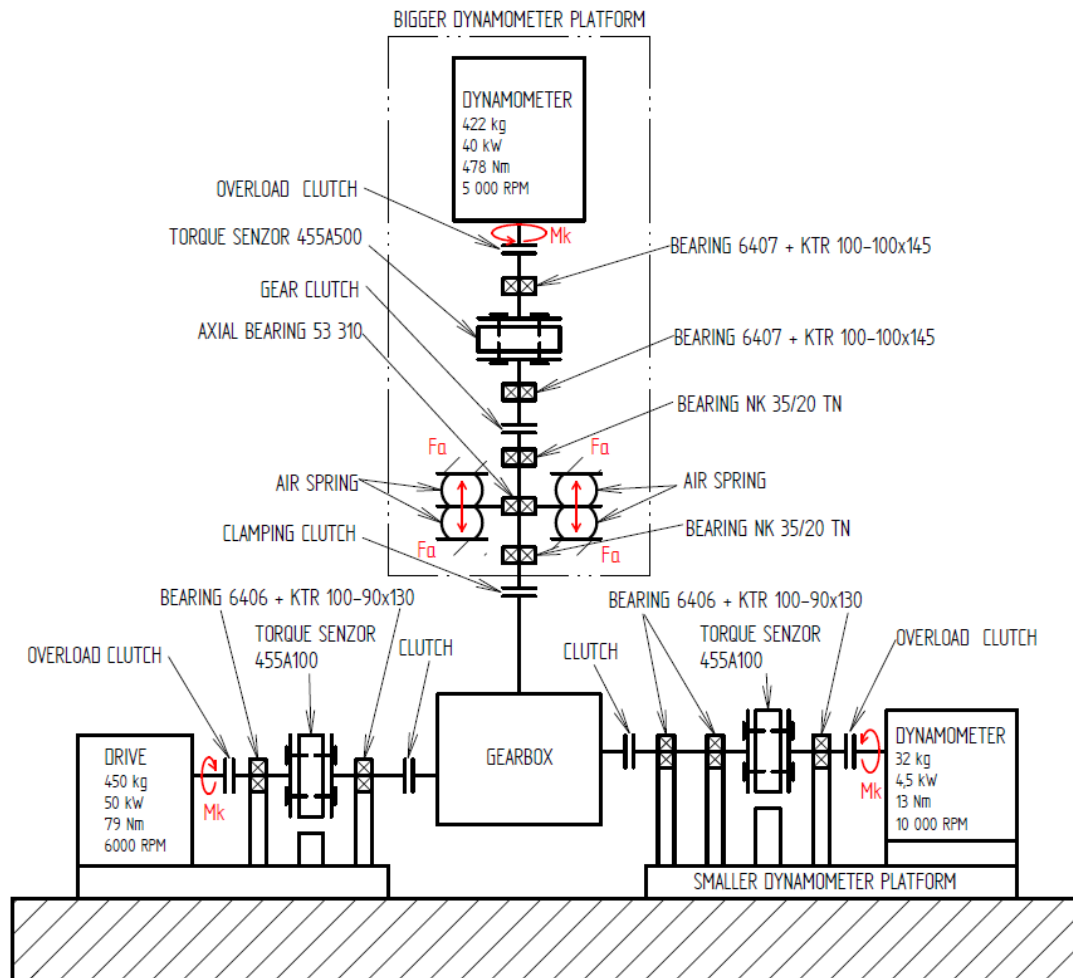
Fig. 1: SkySpotter 150

The company VÚTS cooperates with Modelárna LIAZ on the development of the test station for angular gearboxes. The gearbox is mounted in the helicopter frame in the horizontal position, as shown in Fig. 1. The drones have weight limitations; therefore, the gearbox must be light, but also sufficiently rigid and safe. The gearbox must have a maximum ratio between

weight and power. This cannot be achieved without extensive gearbox testing. Drones have great usage in the world nowadays. SkySpotter 150 should have wide usability in the military service (searching, monitoring, equipment transport and more) but also in the civil sector. The application can be found in firefighter units, geological exploration, rescue works and elsewhere. Its biggest advantage is the possibility to fly under difficult conditions for a long time.

1 Test Rig Design

The schematic diagram of the test rig is shown in Fig. 2. The scheme presents all main components used in the design and their locations. The main parts are a drive, two dynamometers and an axial force mechanism. The strain gauge flange sensors by Kistler are used for torque measurement.



Source: Own

Fig. 2: Schematic diagram of the test rig

The basis of the test rig consists of a welded frame shown in Fig. 3. All main parts are connected to the frame. The frame design allows bigger dynamometer mounting in the vertical or horizontal position, which means it is possible to test other gearbox types with different axis orientation or other helicopter components (for example an engine).



Source: Own

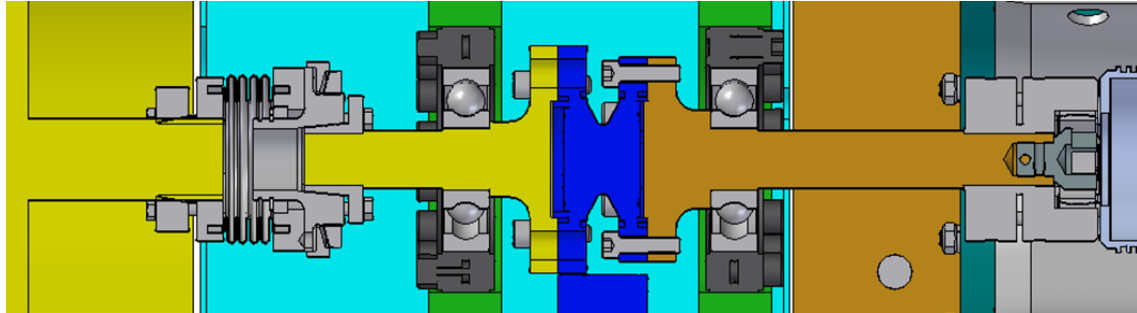
Fig. 3: *The test rig during assembling*

1.1 Drive and Dynamometer

The drive and the dynamometer were supplied by TES Vsetín. The drive is a standard product of this company. It is an asynchronous motor with a maximal power of 50 kW and an external air-cooling. The bigger dynamometer is Siemens asynchronous servomotor working as an electric brake (load). This part has a maximal braking power of 40 kW and it works in the vertical orientation. The dynamometer can work in this position due to a torque measurement realized by an external sensor and the usage of special bearings. The smaller dynamometer is also Siemens asynchronous servomotor, but its maximal power is only 4.5 kW.

1.2 Shaft and Bearings

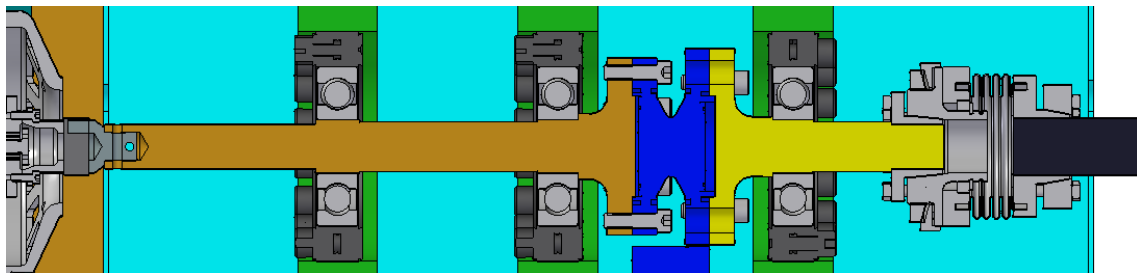
The bearings are mounted through clamping sleeves or directly pressed to parts of the design for the proposed device. The shaft for the drive and the gearbox connection are designed as two parts shown in Fig. 4. The strain gauge flange for torque measurement is mounted between these two parts. A bearing 6406 is pressed on each part of the shaft. Bearings are mounted in clamping sleeves KTR 100 – 90 x 13.



Source: Own

Fig. 4: Shaft connecting drive and gearbox

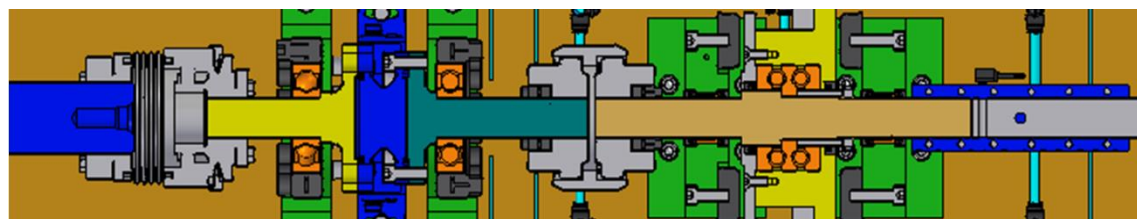
The same solution was used for the shaft connecting the gearbox and the smaller dynamometer shown in Fig. 5. The only difference is in the usage of two bearings on the gearbox side shaft part. Two bearings are used because of the transportation possibility of the independent smaller dynamometer platform.



Source: Own

Fig. 5: Shaft connecting gearbox and smaller dynamometer

The last shaft assembly for connecting the gearbox with the axial force mechanism and the bigger dynamometer in the vertical position is shown in Fig. 6. The shaft between the gearbox and the axial mechanism must enable its axial displacement. It is ensured by two bearings NK 32/20 TN, which are needle bearings without an inner ring. The shaft has a ground surface at the bearing location allowing the axial displacement. These bearings are pressed in parts of the frame. The axial force is transferred via axial bearings 53 310. The shaft between the axial force mechanism and the bigger dynamometer uses the same mounting as the drive shaft. The only difference is the application of larger bearings 6407 and clamping KTR 100 – 100 x 174.



Source: Own

Fig. 6: Shaft connecting axial force mechanism and bigger dynamometer

1.3 Clutches

The gearbox is connected to the test station shafts by the same clutch as in the helicopter. Each shaft has a safety clutch (between the drive or the dynamometers and the torque sensors) ensuring the test station protection against overloading. The safety clutch disconnects the torque when an unexpected condition occurs.



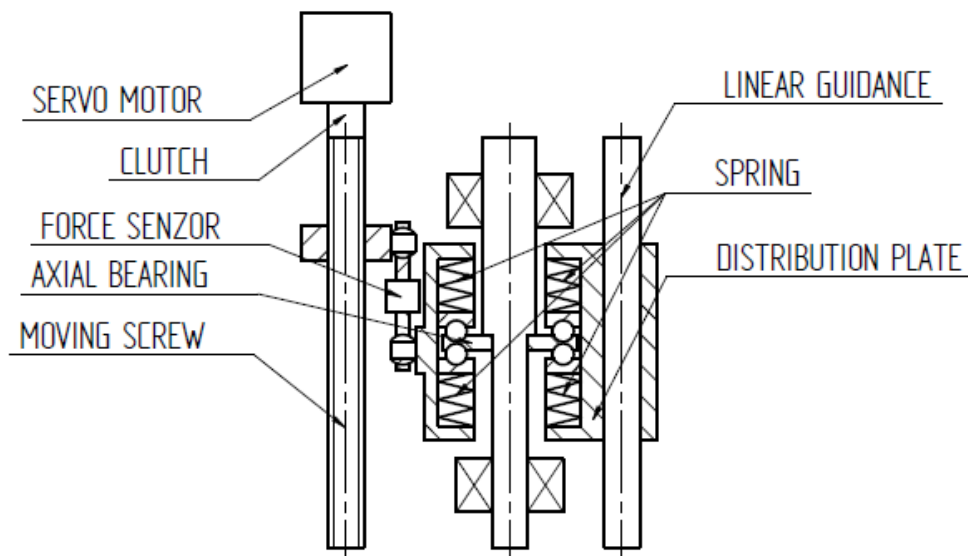
Source: Own

Fig. 7: Gear clutch [2]

An aluminum clamp clutch transfers the axial force from the axial force mechanism to the gearbox output shaft. This material was chosen for the reason the gearbox shaft is undamaging. The clutch between the axial force mechanism and the bigger dynamometer torque sensor does not transfer the axial force because it could damage the torque sensor. Therefore, the gear clutch is used as shown in Fig. 7.

Each clutch was dimensioned for the maximal load of the drive and the dynamometer. The assembly was made by a conical clamping on a smooth shaft.

1.4 Axial Force Mechanism

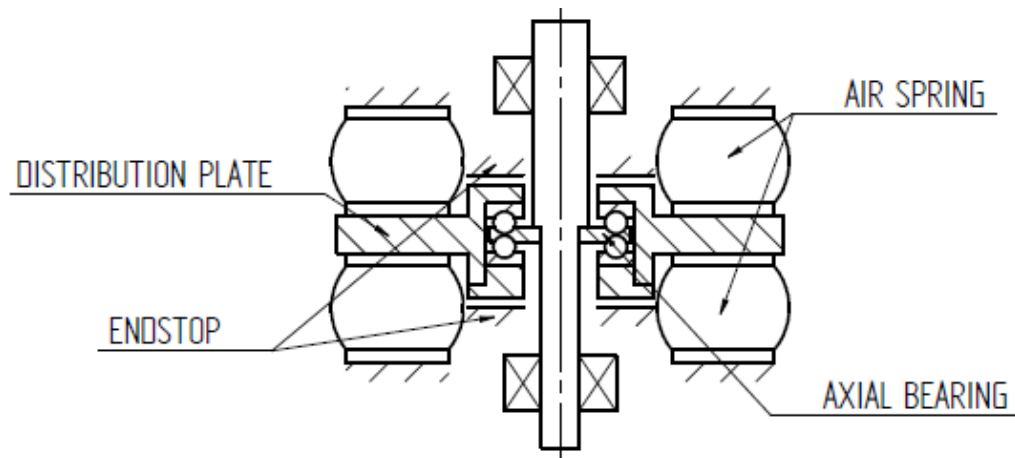


Source: Own

Fig. 8: Version with servomotor

The first draft for the realization of the axial force loading mechanism was proposed for the use of the servomotor. The schematic diagram of this solution is shown in Fig 8. A moving screw driven by the servomotor produces the axial force acting in the axis of the output shaft.

The nut on the moving screw transfers the force to a distribution plate. Appropriate springs should be placed between the nut and the distribution plate because the moving screw angular movement without the springs is close to zero. The disadvantage of this solution is its higher price and complicated design.



Source: Own

Fig. 9: Version with air springs

A new solution with air springs was designed as a cheaper and simpler solution, as it is shown in Fig 9. The air springs directly produce the axial force. All parts of the mechanism must have sufficient stiffness for high force precision and repeatability. An air pressure sensor is connected to supply the circuit of each pair of the air springs. The axial force can be controlled and regulated by a proportional valve; the measured air pressure serves as the feedback signal. The distribution plate position is controlled via a displacement capacitive sensor. A linear guidance is not necessary to use because two pairs of the air springs lead the distribution plate. The mechanism has a mechanical endstop defining dead points of the distribution plate displacement for regimes without the compressed air and/or too big pressure.

Conclusion

Development and design of the test station for angular gearboxes with axial force and torque load is presented. This solution is primarily focused on testing of gearboxes used in unmanned helicopter developed by Modelárna LIAZ company. The test station can load the gearbox by defined torque and axial force on the output shaft and simultaneously measures actual values of torque, angular speed, axial force, vibrations, temperature and noise.

Acknowledgements

This work was supported by the Czech Ministry of Industry and Trade in the framework of the TRIO program.

Literature

- [1] LIAZ: *SkySpotter 150 UAV system*. [online]. Available from WWW: <https://www.liaz-uav.com>
- [2] LENZE SELECTION: *Zubové spojky – mechanické*. [online]. [accessed 2022-02-25]. Available from WWW: <https://www.lenze-selection.com/cs-cz/vyrobky/spojky-hridelove-prirubove-spojky/zubove-spojky/>

Ing. Jan Bělík

TESTOVACÍ ZAŘÍZENÍ PRO PŘEVODOVKY VRTULNÍKU SKYSPOTTER 150

Bezpilotní vrtulník SkySpotter 150 je vyvinut firmou Modelárna LIAZ. Testovací zařízení pro převodovky vrtulníku nejsou standartní pracoviště. Je zde pohon provázaný s dynamometrem a axiálním zatěžovacím mechanismem simulujícím zatížení od rotoru na výstupním hřídeli převodovky. Proto je potřeba speciálního pracoviště. Byl navržen měřicí řetězec včetně jednotlivých snímačů a konstrukce se speciální orientací dynamometru. Konstrukce má bezpečnostní prvky, které chrání testovací zařízení a její obsluhu. Testovací pracoviště je využito k vývoji nových generací vrtulníku. Dále slouží k ověřování parametrů nových převodovek, ale i k technické diagnostice převodovek při opakovaných kontrolách.

TESTANLAGE FÜR DIE GETRIEBE DES HUBSCHRAUBERS SKYSPOTTER 150

SkySpotter ist ein unbemannter Hubschrauber und wurde von der Firma Modelárna LIAZ entwickelt. Bei der Testanlage für die Getriebe des Hubschraubers handelt es sich um keinen Standardarbeitsplatz. Hier wird der Antrieb mit einem Dynamometer und einem Belastungsmechanismus verbunden, wobei der Belastungsmechanismus eine Belastung vom Rotor auf die Ausgangswelle des Getriebes simuliert. Daher bedarf es eines speziellen Arbeitsbereichs. Es wurden eine Messkette inklusive einzelner Abtaster sowie eine Konstruktion mit einem speziellen Orientierungsdynamometer entworfen. Die Konstruktion verfügt über Sicherheitselemente, welche die Testanlage und deren Bedienung schützt. Die Testanlage wird zur Entwicklung neuer Helikoptergenerationen genutzt. Weiter dient sie zur Überprüfung der Parameter neuer Getriebe, aber auch zur technischen Diagnostik der Getriebe bei wiederholten Kontrollen.

STANOWISKO BADAWCZE PRZEKŁADNI ŚMIGŁOWCA SKYSPOTTER 150

SkySpotter 150 to bezzałogowy śmigłowiec opracowany przez firmę Modelárna LIAZ. Stanowiska badawcze przekładni śmigłowca nie mają standardowej konstrukcji. Napęd jest połączony z dynamometrem i mechanizmem obciążenia osiowego, który symuluje obciążenie głównego wirnika na wale wyjściowym przekładni. Z tego powodu potrzebne jest zastosowanie specjalnego stanowiska. Opracowano tor pomiarowy obejmujący poszczególne czujniki oraz konstrukcję ze specjalnie ukierunkowanym dynamometrem. Konstrukcja posiada elementy bezpieczeństwa, które chronią stanowisko badawcze i jego obsługę. Stanowisko badawcze jest wykorzystywane do projektowania śmigłowców nowej generacji. Ponadto służy ono również do weryfikacji parametrów nowych przekładni, a także diagnostyki technicznej przekładni podczas przeglądów okresowych.

SCREW SORTING APPLICATION WITH 6 DoF UR5E ROBOT ARM

**Hamid Castillo Martinez¹; Emiliano Lara Romero²; Ricardo Ugalde Tinoco³;
Christian Vogel⁴**

Zittau/Görlitz University of Applied Science,
Faculty of Electrical Engineering and Informatics,
Institute of Process Technology, Process Automation and Measurement Technology
Theodor-Körner-Allee 16, 02763, Zittau, Germany

e-mail: ¹hamid_omar.castillo_martinez@stud.hszg.de; ²emiliano.lara_romero@stud.hszg.de;
³ricardo.ugalde_tinoco@stud.hszg.de; ⁴c.vogel@hszg.de

Abstract

As part of the module “Introduction of Collaborative Robot Systems” at the Zittau/Görlitz University of Applied Sciences, a practical robot application using a collaborative robot and the associated human-robot interaction must be examined in a written document. The objective of the document is to design an application for sorting screws in such a way that the motion sequences of the robot are optimized. Safety aspects are to be considered. Subsequently, the concept is to be implemented theoretically and/or practically. The work carried out and the results are to be recorded in a document. In this article, the results of the proof of a student group are presented. Thereby, the article shall give an overview on the possible procedure for the conceptual design of practical robot applications.

Keywords

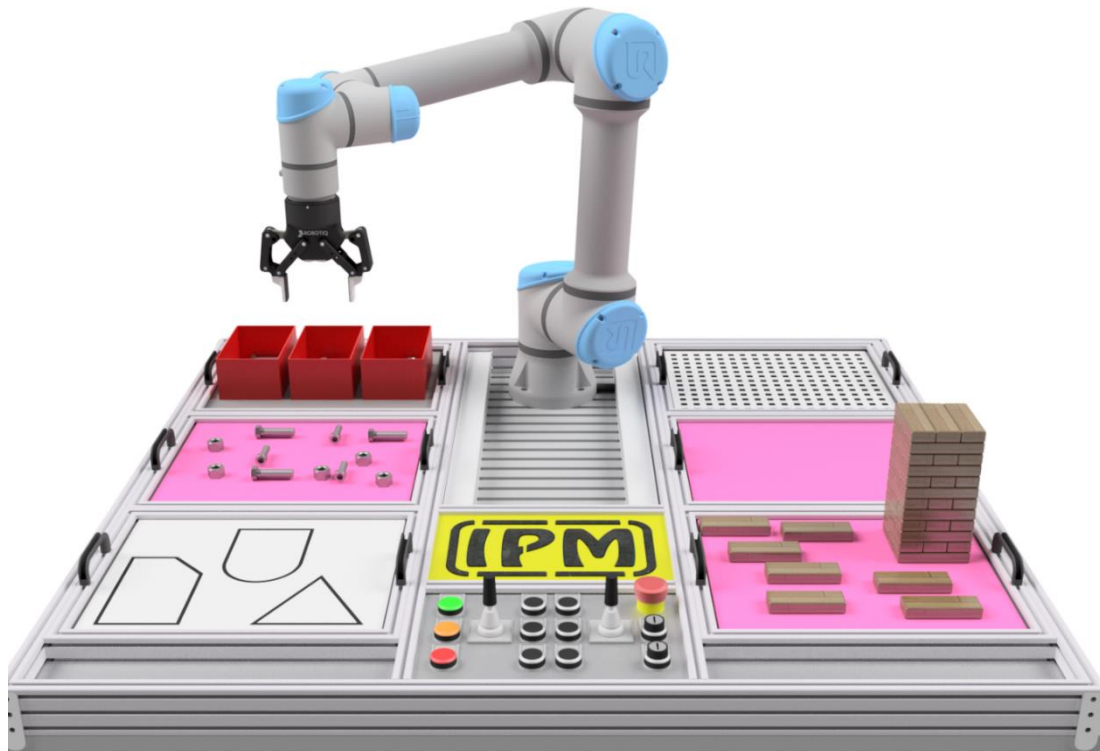
Human-robot interaction; Collaborative robots; Robot application; Sorting; Screwing; Teaching.

Introduction

Small and medium-sized enterprises (SME) form the basis for a functioning and innovative economy in Germany, but SME are increasingly confronted with social and economic challenges. The social challenges include, for example, demographic change with a declining number of people of working age and the associated shortage of skilled workers. The economic challenges include, for example, steadily increasing international market pressure, rising demand, declining product life cycles and greater diversity of variants. These challenges mean that previously fully automated or manual production processes are becoming increasingly complex. As a rule, fully automated production systems have the characteristic of high productivity but low flexibility, and manual production systems have the characteristic of high flexibility but low productivity. One way of maintaining economic efficiency and counteracting the shortage of skilled workers in industry and the skilled trades is to use hybrid production processes, thus combining the properties of productivity and flexibility. A key technology of future hybrid production environments is the human-robot interaction (HRI) by means of collaborative robots. [1]

The following article presents the conceptual design of an application for sorting screws by means of a collaborative robot, in which humans continue to be part of the process. The goal is the development of a complete sorting routine on the given training platform of the Institute of Process Technology, Process Automation and Measurement (IPM) at the University of

Applied Sciences Zittau/Görlitz with the collaborative robot UR5e of the company Universal Robots. The training platform is shown in Figure 1.



Source: Own

Fig. 1: Training platform for the UR5e collaborative robot from Universal Robots

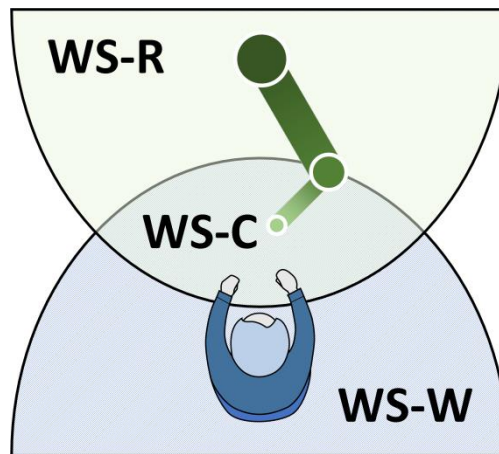
The application includes the classification of three different types of screws. The focus of this work is on the presentation of a possible variant of the sorting application, the improvement of the cycle time by optimized motion sequences of the robot as well as a possible integration of safety measures to protect the worker. The identification of the screw type as well as the position in the system by means of methods of image processing and artificial intelligence are not the subject of this work. Rather, the synergy between CAD, CAE, simulation and process management is to be presented.

A CAD model of the training platform serves as a reference for the various coordinate points of the application, which are used as waypoints for the theoretical implementation of the complete routine. The routine is implemented in the simulation software URSim from Universal Robots. URSim is used for offline programming as well as simulation of the created robot program. The results are analyzed and conclusions are derived.

1 Basics

In general, HRI distinguishes between three forms of interaction. For this purpose, it is first necessary to define the possible workspaces in an HRI. Figure 2 shows three possible workspaces:

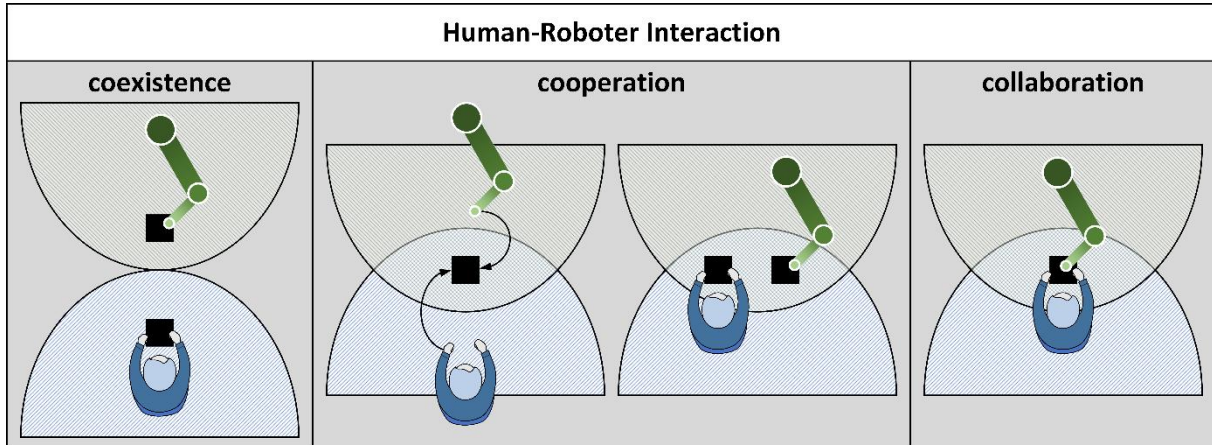
- Workspace of the worker (WS-W),
- workspace of the robot (WS-R), and
- common workspace for worker and robot (WS-C).



Source: Own

Fig. 2: Definition of the workspaces in a human-robot interaction

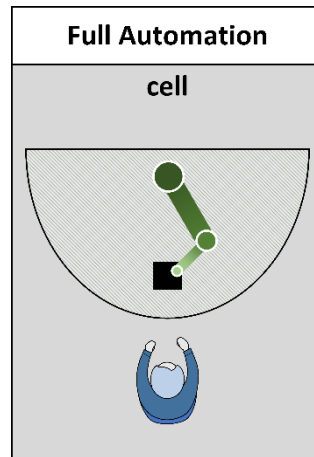
The possible forms of interaction between worker and robot are shown in Figure 3. In the case of coexistence, the worker and robot work side by side and do not have a common workspace, i.e. the worker and robot work alone in their respective workspaces. The interaction form cooperation is distinguished in two variants. In the first variant (left), the worker and the robot have a common workspace, but they are separated in time, i.e. only one interaction partner is active in the common workspace at any given time. In the second variant (right), the two interaction partners interact simultaneously in the shared workspace, but the interaction partners do not work on the same component at the same time. The last form of interaction is collaboration, in which both interaction partners work on the same component at the same time.



Source: [2]

Fig. 3: Forms of interaction between worker and robot

There is another special form in which a collaborative robot is used. This special form is full automation, i.e. the robot interacts alone in a cell without the worker being directly involved in the production process. Figure 4 shows full automation as a special form of interaction.



Source: [2]

Fig. 4: Full automation as a special form of human-robot interaction

Collaboration-capable robots were developed for direct physical interaction between worker and robot. The actual use of collaborative robots is in assembly for ‘slow’ processes with low payloads and low process forces and serves to support and relieve the worker. The collaborative robot is a sub-component of a robotic system, i.e. for a complete robotic system it is necessary to add an end effector and the necessary peripherals and accessories to the collaborative robot to support the intended application. The end effector is the final link in a robot’s kinematic chain. Here, end effectors are subdivided into grippers, tools and measuring or testing equipment.

In addition to selecting a suitable end effector for the respective application, it is also necessary to select a suitable collaborative robot. For the selection of a suitable collaborative robot, various properties and parameters are used, such as degrees of freedom, working space, accuracy, payload and price. For the further considerations, the collaborative robot UR5e from the company Universal Robots is taken.

Universal Robots is a company in charge of developing collaborative robots. This enterprise was developed in Denmark. The most popular product of this company is the six-jointed robot arms. There are only seven different types of six-jointed robot arms: UR3, UR3e, UR5, UR5e, UR10, UR10e, and UR16. [3] Figure 5 shows the e-Series collaborative robots from Universal Robots.



Source: [4]

Fig. 5: Models of six-joint robot arms from Universal Robots

The UR5e is a 6-axis robotic arm produced by Universal robots, with some important aspects like an error ranging from a ± 0.1 mm mark, a maximum payload of 5 kg, a reach of 850 mm, and a working temperature range that goes from 0 to 50 °C. [5]

The type and model of the robot is not the only important feature for developing the project, but also choosing the accurate gripper and camera for image processing is of grave importance, that is why in the following paragraphs, the characteristics of the gripper and the camera we choose will be given. Table 1 summarizes the characteristics of the gripper used. Figure 6 shows the gripper used by the company Robotiq.

Tab. 1: *Gripper specifications*

Specifications	2F-140
Stroke (Adjustable)	140 mm
Grip force (Adjustable)	10 to 125 N
From-fit grip payload	2.5 kg
Friction grip payload	2.5 kg
Gripper Mass	1 kg
Position resolution (fingertip)	0.6 mm
Closing Speed	30 to 250 mm/s
Communication Protocol	Modbus RTU (RS-485)
Ingress Protection (IP) rating	IP40

Source: [6]



Source: [6]

Fig. 6: *Gripper 2F-140*

Figure 7 shows the flange camera from the company Robotiq. Table 2 summarizes the characteristics of the used 2D camera.



Source: [7]

Fig. 7: *Wrist Camera from Robotiq*

Tab. 2: Camera specifications

Specifications	Wrist Camera
Sensor and optics	5 MP color sensor, electrically adjustable focus, 70 mm to infinity
Integrated lighting	Two units (white and diffuse LED)
Programmable parameters	<ul style="list-style-type: none">- Automatic part programming (user-defined arbitrary shape)- Parametric part programming (circle, ring, square, rectangle)- Edge editing, color validation- 2 convenient camera control modes: basic, advanced- Automatic and manual camera parameters: exposure, focus, illuminationLED, white balance
Electric	Direct communication with the UR controller (via USB), and power supply from the controller (24 V).
Weight	160 g
Working temperature	0 – 50 °C
Internal camera image buffer	DRAM memory

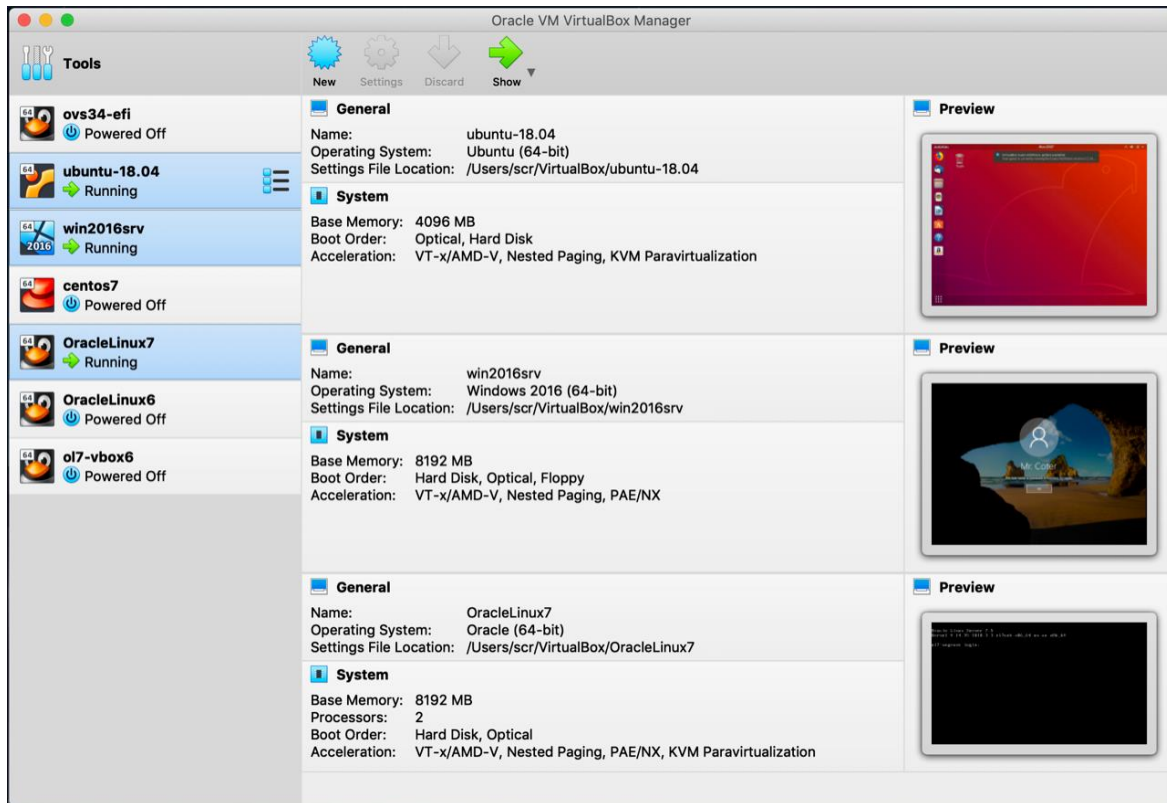
Source: [7]

VirtualBox is a powerful x86 and AMD64/Intel64 virtualization product for enterprise as well as home use, it is installed on your existing Intel or AMDbased computers, whether they are running Windows, Mac OS X, Linux, or Oracle Solaris operating systems (OSes). It extends the capabilities of your existing computer so that it can run multiple OSes inside multiple virtual machines at the same time. [8]

This software offers the following advantages:

- Host operating system (host OS).
- Guest operating system (guest OS).
- Virtual machine (VM).

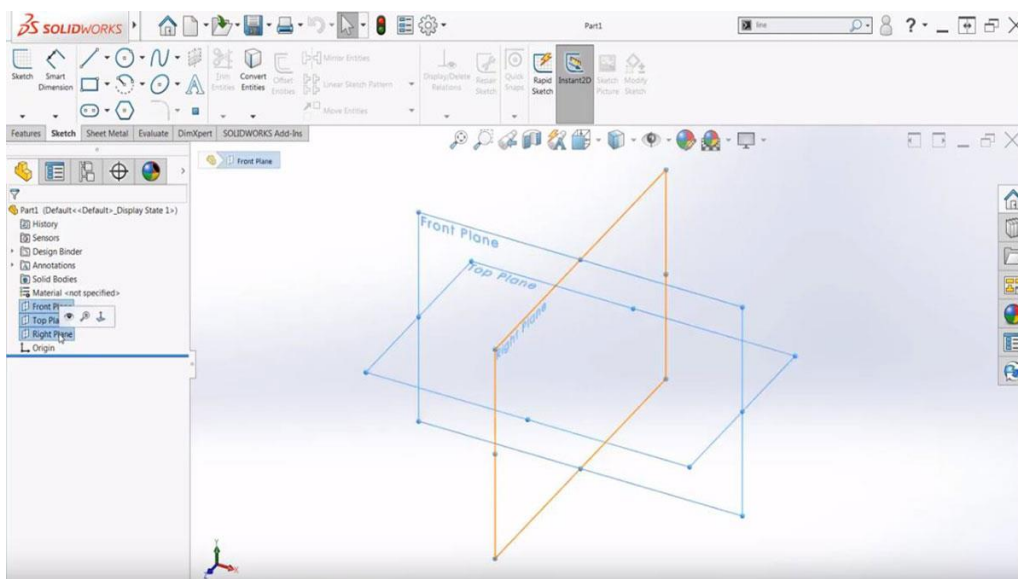
Figure 8 shows the virtual machine interface. There it is possible to select a defined operating system.



Source: [9]

Fig. 8: Virtual Box interface







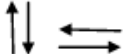
SolidWorks is computer-aided design software that allows users to create, simulate, publish, and manage 3D models. The technique generally consists of making 2D profile sketches and then using methods to produce the solid shape, be it extrusion, revolution, rounding, chamfering, etc. This allows for the creation of a 3D model (solid or surface), to finally create assemblies with different parts, using geometric relationships. This software was developed by SolidWorks Corp. a subsidiary of Dassault Systèmes, in 1995 in Massachusetts. [10] Figure 9 shows the SolidWorks user interface.



Source: [11]

Fig. 9: SolidWorks interface

A flowchart is a diagram that describes a process, system, or computer algorithm. They are widely used in numerous fields to document, study, and plan, improve and communicate often complex processes in clear, easy-to-understand diagrams. Flowcharts employ rectangles, ovals, diamonds, and numerous other shapes to define the type of step, along with connecting arrows that establish the flow and sequence. They can range from simple, hand-drawn diagrams to comprehensive, computer-created diagrams that describe multiple steps and paths. Figure 10 shows and describes some symbols of the flowchart. [12]

Symbol	Name	Function
	Process	Indicates any type of internal operation inside the Processor or Memory
	input/output	Used for any Input / Output (I/O) operation. Indicates that the computer is to obtain data or output results
	Decision	Used to ask a question that can be answered in a binary format (Yes/No, True/False)
	Connector	Allows the flowchart to be drawn without intersecting lines or without a reverse flow.
	Predefined Process	Used to invoke a subroutine or an Interrupt program.
	Terminal	Indicates the starting or ending of the program, process, or interrupt program
	Flow Lines	Shows direction of flow.

Source: [13]

Fig. 10: Flow chart symbols

As this is a very regulated technique, there are some rules for developing a correct Flow chart, which are the following:

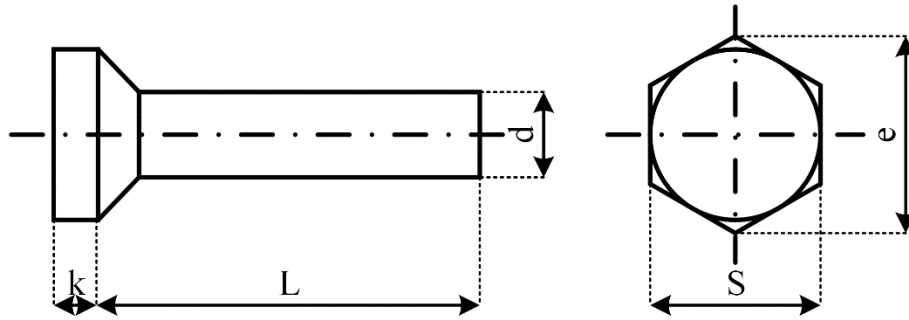
- (1) All boxes of the flowchart are related with arrows.
- (2) Flowchart symbols have an entry point on the top of the symbol with no other entry points. The exit point for all flowchart symbols is on the bottom except for the decision symbol.
- (3) The decision symbol has two exit points; these can be on the sides or the bottom.
- (4) Generally, a flowchart will flow from top to bottom.
- (5) Connectors are used to join breaks in the flowchart.
- (6) All flowcharts end with a terminal or a continuous loop.
- (7) Subroutines and interrupt programs have their own and independent flowcharts.

In order to successfully complete the development of the Flowchart, the software EdrawMax was used.

2 Concept

During the development of the concept, our main purpose is the pick and place application of a variety of screws from a pile to a specific box in concrete numbers; this statement can be oversimplified in broad steps to establish an order of operation from which more specific instructions will take place.

Before the core part of this article, the screws used are described. For this purpose, a bolt and its definitions are shown in Figure 11.



Source: [14]

Fig. 11: Screw Schematic

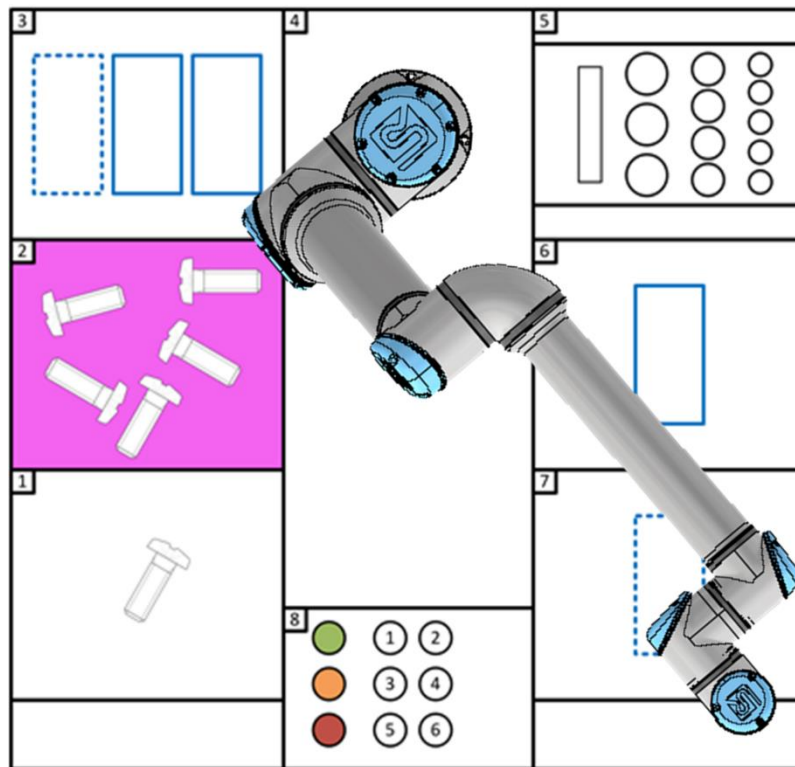
Table 3 summarizes the screws used and their parameters.

Tab. 3: Screw Selection

	M18	M20	M24
k [mm]	11.5	12.5	15.0
S [mm]	27.0	30.0	36.0
L [mm]	100.0	100.0	100.0
Norm	DIN 933	DIN 933	DIN 933

Source: [14]

The next section will define in multiple steps the timeline of the process that takes place to be able to later program everything in the robot. It will also define some of the considerations that we have laid in and that define the boundaries, limitations, and givens of our project. Figure 12 shows the basic structure of the application. Section 2.1 describes the individual positions and the functional sequence.



Source: Own

Fig. 12: Training platform arrangement

2.1 Functionality Description

The robot is in the HOME position.

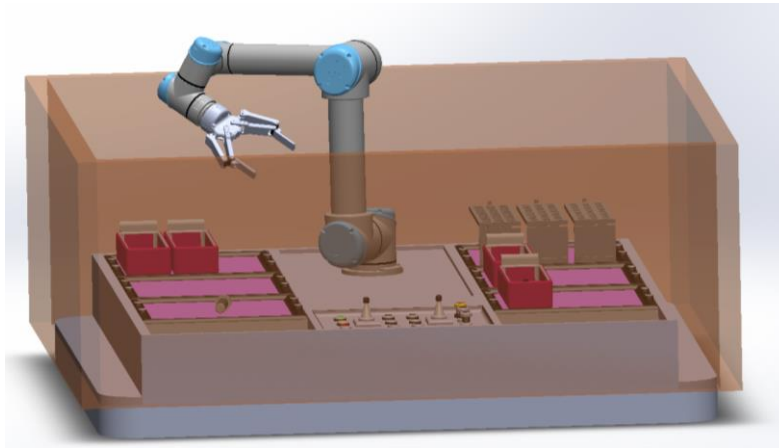
The outside operator loads the varieties of screws in section 2.

The robot goes to section 2.

- (1) The robot selects a screw from the pile.
- (2) The robot places the screw in the correct position in section 5.
- (3) The steps (3), (4), and (5) are repeated until all the racks on section 5 are full.
- (4) The robot takes an empty box from section 3.
- (5) The robot places the box in the correct spot in section 6.
- (6) Steps (7) and (8) are repeated placing a total of 3 boxes in section 6.
- (7) The robot takes the racks from section 5.
- (8) The robot empties the screws on the boxes in section 6.
- (9) The robot leaves the empty racks in section 5.
- (10) The robot takes a full box in section 6.
- (11) The robot leaves a full box in section 7.
- (12) Steps (13) and (14) are repeated for the 3 boxes.
- (13) The robot notifies the operator that the boxes in section 7 are ready to take away.

3 Safety

After examination of the possible failure scenarios and reviewing the theoretical concepts for correct practice, the most accurate action is to introduce the planes of security and define a safety sphere that covers the screw; this plane will be allocated 5 cm after the border of the base. This way, the robotic arm has more space for developing the movements of the routine and at the same time avoiding the cylinder of singularities. This position also circumvents a collision with the operator, while he is passing by or introducing the screws in the first area. In addition, a presence sensor will be installed in front of the first area and another next to the eighth area described below. With these sensors, the speed of the robot will be reduced when the operator introduces his hand to place more screws, this way the robot will be maintained steady when the boxes are full of screws. Figure 13 shows the safety planes of the application with the robot.

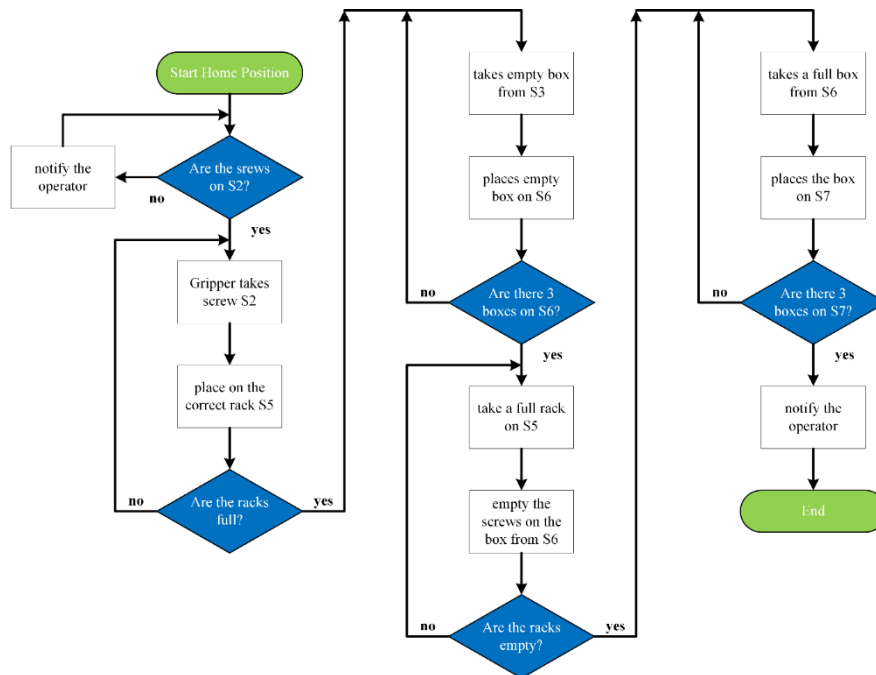


Source: Own

Fig. 13: Safety Planes

4 Program Flowchart

Figure 14 shows and describes the flowchart of the application process.

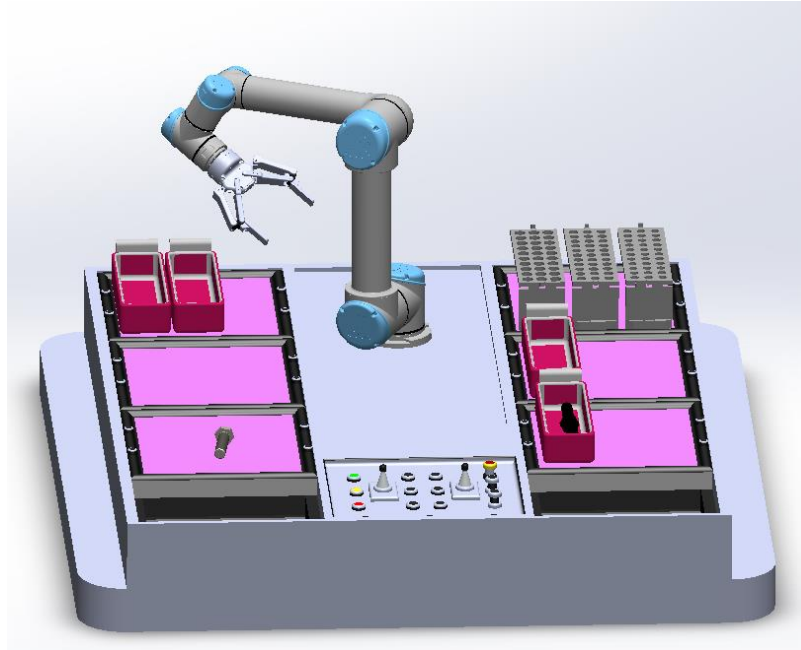


Source: Own

Fig. 14: Process Flowchart

5 Summary

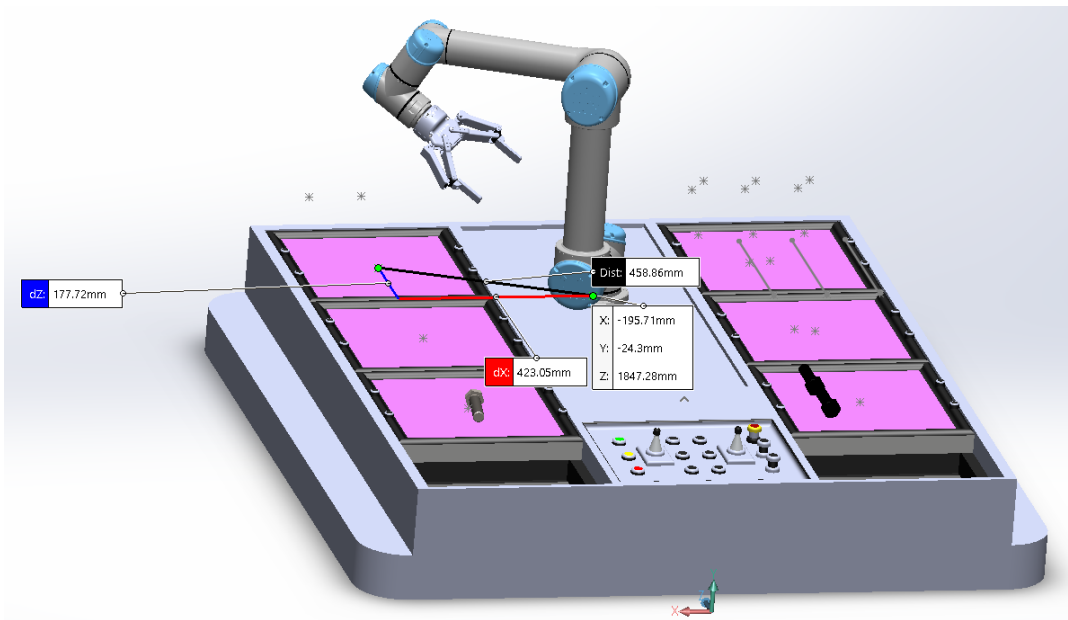
For this activity, a 3D simulation in Solid Works was created to simulate a more realistic scenario, in which a square workspace of 1.5 meters was assigned, divided as shown in the instructions. Figure 15 shows the 3D model of the application with the robots.



Source: Own

Fig. 15: 3D Simulation of the Process

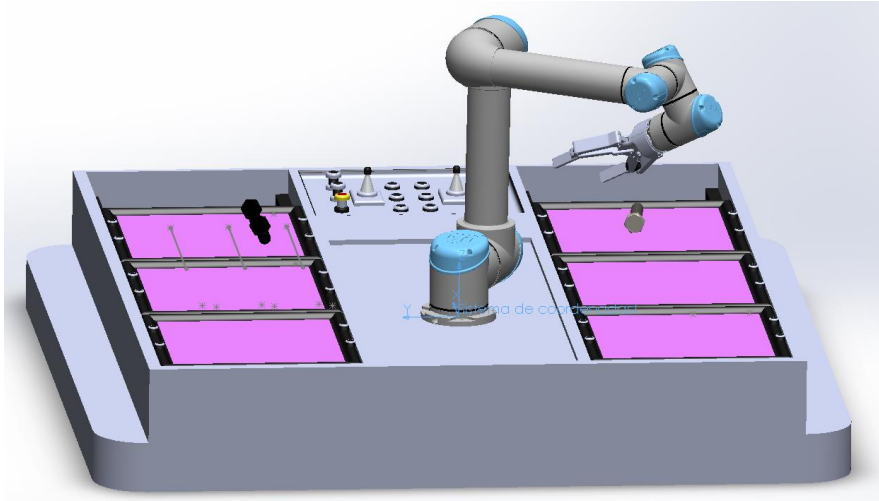
Once the 3D simulation was completed, distances from each of the allocations of the pick and place points were taken with the distance tool, as shown in figure 16.



Source: Own

Fig. 16: Coordinates of the interest points

To make the process of acquisition of the points easier, a new axis system in the base of the UR5e was created since the coordinates in the software begin at the base of the robot. Figure 17 shows the application with the robots and the new coordinate system.



Source: Own

Fig. 17: New coordinate system

Once the coordinate points were taken from the model, the distances were introduced in the Universal Robots software to create the program, considering the accurate movements for moving, picking, and placing. While launching the application it was seen that for the completion of one screw, the robot took 6 minutes. For that reason, optimization curves were introduced, and an increase to the speed of the robot. With both of those changes, time was reduced from 6 minutes to 5 minutes and 17 seconds.

Despite the important decrease of time, optimization was further needed in the simulation; that is why a spring system was installed in the racks, this would allow the robot to make a single movement instead of two. With this approach, another minute was saved. Finally, an analysis of the decision points given in the Flowchart was implemented in the program.

An additional step was made to capture a simulation of the program in the Virtual Box. For this purpose, the video conferencing application of Zoom fulfilled that motive. A video of the created program can be found in [15]. Figure 18 shows a QR code that redirects to YouTube. The video on YouTube shows the simulation of the application in the virtual machine.



Source: Own

Fig. 18: Virtualbox video QR

Conclusion

Considerations for industry standards must be included for the application to successfully achieve the routing, sorting, and packing application for different types of screws. They will trace the guidelines and rules to be followed for a proper application.

Limitations regarding software components made some concept implementations problematic to implement and place in the virtual machine. Enactment of the described work would have provided more data to analyze weak points of the theoretical application. In terms of this scope, further examination is required for the wired connections to the robot arm and the accurate functionality of the gripper. Nevertheless, the described theoretical application may be used as a basis for an industrial level application with similar proposed parameters.

One of the main objectives was the further optimization of the process even when it was already constrained by programming factors. For example, the system of springs installed in the rack helps the operator to program the first movement to place the screws in the box and the spring itself returns the rack to its place, this way movements and times are reduced.

Additionally, research for different types of grippers was made to obtain information about the ones available in the market which would fit best for the application. Filters were applied to the selection depending on their dimensions, costs, and functionalities. The chosen gripper was the 2F-140 because of its cost compared to the other options, its good traction and its shape that allows for thrift of movements to avoid changing the directions for picking and placing. On the other hand, the selection of the camera depended on the selection of the gripper. This was due to a lack of information regarding a handful of deep learning cameras that would be suited for the application. The only way for a camera to be integrated into the arm of the robot itself was only if a combination of both was selected.

The functionality of the camera and its image processing capabilities were indirectly given in the code, but a written description of it was not added. A practical approach would have made the configuration introduced to the code in the Universal Robots program much clearer by using the camera as an input. Given the scope and approach of this investigation, it was left implicitly.

Since the theoretical basis of the enactment of the 6DoF robot arm for the screw sorting application has enough descriptions and meets the considered optimization objectives, it can be stated that the routine is complete, and it now can be used as the basis in an industrial sorting application.

Acknowledgments

We would like to thank Ing. Christian Vogel, for guiding us in the creation of this article and for the theory provided for the development of this article.

Literature

- [1] SCHLEICHER, T.: Kollaborierende Roboter anweisen – Gestaltungsempfehlungen für ergonomische Mensch-Roboter-Schnittstellen. Springer, Leipzig, 2020. ISBN 978-3-658-29050-4. eBook ISBN 978-3-658-29051-1. DOI: [10.1007/978-3-658-29051-1](https://doi.org/10.1007/978-3-658-29051-1)
- [2] BAUER, W.; BENDER, M.; BRAUN, M.; RALLY, P.; SCHOLTZ, O.: Roboter ohne Schutzzaun in der Montage: Stand der Anwendung in deutschen Montagen. *wt Werkstattstechnik online*. 2016. DOI: [10.37544/1436-4980-2016-09-42](https://doi.org/10.37544/1436-4980-2016-09-42)

- [3] ASSOCIATION FOR ADVANCING AUTOMATION: *Universal Robots A/S*. [online]. 2012. [accessed 2021-06-15]. Available from WWW: <https://www.automate.org/companies/universal-robots-a-s>
- [4] SAMSYS GmbH: *Universal Robots e-Serie*. [online]. 2019. [accessed 2021-06-15]. Available from WWW: https://www.samsys.eu/product/universal_robots/
- [5] CLEARPATH: *UR5*. [online]. 2021. [accessed 2021-06-15]. Available from WWW: <https://store.clearpathrobotics.com/products/universal-robots-ur5>
- [6] ROBOTIQ: *2F-85 and 2F-140 Grippers*. [online]. 2021. [accessed 2021-06-15]. Available from WWW: <https://robotiq.com/products/2f85-140-adaptive-robot-gripper>
- [7] ROBOTIQ: *Wrist Camera*. [online]. 2021. [accessed 2021-06-15]. Available from WWW: <https://robotiq.com/products/wrist-camera>
- [8] ORACLE: *Virtual Box*. [online]. 2021. [accessed 2021-06-17]. Available from WWW: <https://www.virtualbox.org>
- [9] ORACLE: *Virtual Box: Chapter 1.6. Starting Oracle VM VirtualBox*. [online]. 2021. [accessed 2021-06-17]. Available from WWW: <https://www.virtualbox.org/manual/UserManual.html#intro-starting>
- [10] CAPITOL TECHNOLOGY UNIVERSITY: *What is SOLIDWORKS?* [online]. 2019. [accessed 2021-06-18]. Available from WWW: <https://www.captechu.edu/blog/solidworks-mechatronics-design-and-engineering-program>
- [11] AMES, J.: *User Interface Basics in SOLIDWORKS*. [online]. USA, California, Hawk Ridge Systems, 2019. [accessed 2021-06-18]. Available from WWW: <https://hawkridgesys.com/blog/user-interface-basics-in-solidworks>
- [12] WONDERSHARE EDRAW MAX: *What is a Flowchart: A Complete Guide*. [online]. 2021. [accessed 2021-06-19]. Available from WWW: <https://www.edrawmax.com/flowchart/>
- [13] KANDWAL, N.: *Flowchart*. [online]. 2021. [accessed 2021-06-19]. Available from WWW: http://naveenkandwal.blogspot.com/2014/01/flowchart_18.html
- [14] GESTIÓN DE COMPRAS: *Screws*. [online]. 2021. [accessed 2021-06-19]. Available from WWW: https://www.gestiondecompras.com/files/products/mechanical_components_hardware/pernos_tornilleria_tuercas_arandelas_varilla_roscada_din_933_934_7989_125_127_403_4_975_555_iso.pdf
- [15] UGALDE, R.: *Screw Sorting Application*. [accessed 2021-06-11]. Available from WWW: https://www.youtube.com/watch?v=ep2sLfHYcn4&ab_channel=RicardoUgalde

Hamid Castillo Martinez; Emiliano Lara Romero; Ricardo Ugalde Tinoco;
Ing. Christian Vogel

APLIKACE TRÍDĚNÍ ŠROUBŮ S ROBOTICKÝM RAMENEM UR5E SE 6 STUPNI VOLNOSTI

V rámci modulu „Úvod do kolaborativních robotických systémů“ na Vysoké škole aplikovaných věd v Žitavě/Görlitz je třeba písemně zpracovat praktickou aplikaci robota s využitím kolaborativního robota a související interakci člověka s robotem. Cílem dokumentu je navrhnout aplikaci pro třídění šroubů tak, aby byly optimalizovány pohybové sekvence robota. Je třeba zohlednit bezpečnostní aspekty. Následně je třeba tento koncept teoreticky a/nebo prakticky realizovat. Provedené práce i výsledky se zaznamenávají do dokumentu. V tomto článku jsou uvedeny výsledky důkazu skupiny studentů. Dokument by měl poskytnout přehled možného postupu při koncepčním návrhu praktických robotických aplikací.

SCHRAUBENSORTIERAPPLIKATION MIT 6 FREIHEITSGRADEN UR5E-ROBOTERARM

Im Rahmen des Moduls „Introduction of Collaborative Robot Systems“ an der Hochschule Zittau/Görlitz ist es als Prüfungsleistung erforderlich eine praxisnahe Roboteranwendung unter Einsatz eines kollaborationsfähigen Roboters und die dazugehörige Mensch-Roboter-Interaktion in einem schriftlichen Beleg zu betrachten. Die Zielstellung des Beleges ist es, eine Anwendung zum Sortieren von Schrauben so zu konzeptionieren, dass die Bewegungsabläufe des Roboters optimiert sind. Dabei sollen sicherheitstechnische Aspekte berücksichtigt werden. Anschließend soll das Konzept theoretisch und/oder praktisch umgesetzt werden. Die durchgeführten Arbeiten sowie die Ergebnisse sind in einem Beleg festzuhalten. In diesem Beitrag werden die Ergebnisse des Beweises einer studentischen Gruppe vorgestellt. Dabei soll der Beleg einen Überblick zum möglichen Vorgehen zur Konzeptionierung von praxisnahen Roboteranwendungen geben.

APLIKACJA SORTOWANIA ŚRUB Z RAMIENIEM ROBOTYCZNYM UR5E O 6 STOPNIACH SWOBODY

Celem niniejszego artykułu jest przedstawienie rozwoju pełnej procedury sortowania na platformie Universal Robots dla modelu UR5e, w której sortowane są trzy różne typy śrub, które są przyporządkowane do różnych, wcześniej ustalonych etapów. Model CAD jest udostępniony jako odniesienie do różnych punktów współrzędnych zastosowania, które mają być użyte jako punkty orientacyjne w symulacji Virtual Box w celu zaprogramowania pełnej procedury a następnie wyciągnięcia wniosków na podstawie analizy wyników.

MODELING OF THE TEMPORAL BEHAVIOR OF THE SURFACE TEMPERATURE OF AN ISOLATION MATERIAL TEST SAMPLE UNDER AN AC LOW CURRENT ARC

Daniel Fiß¹; Stefan Kühnel²; Ernest Krzyszkowski³; Stefan Kornhuber⁴

Hochschule Zittau/Görlitz, University of Applied Science,

^{1,3} Institute of Process Technology, Process Automation and Measurement Technology (IPM)
Department Measuring Technology / Process Automation

^{2,4} Faculty of Electrical Engineering and Informatics
Department for High-Voltage Engineering / Materials / Electromagnetic Theory

Theodor-Körner-Allee 16, 0273, Zittau, Germany

e-mail: ¹d.fiss@hszg.de; ²s.kuehnel@hszg.de; ³ernestkk1996@gmail.com;
⁴s.kornhuber@hszg.de

Abstract

In this article, a computational model is presented which can be used to predict the heating of insulating material surfaces by low-current high-voltage arcs. The discharge is represented by a so-called three-cylinder model. Based on this, the heat flows onto the insulating material surface and its heating by means of thermal conduction and convection are calculated. The calculation results are compared to the measurements of the surface temperature on a model arrangement. The overall model reproduces the dynamic behavior of the heating very well. The quantitative deviations from the measurement are only in the range of a few percent.

Keywords

Low current high voltage arcing; Modeling; Heating of insulating material surfaces; Electrical polymer insulating materials; Arc resistance.

Introduction

The use of polymeric insulating materials as housing materials for components in medium and high voltage applications is widespread. These offer various advantages compared to glass or porcelain components [1]. When polymeric insulating materials are used for outdoor applications, they are exposed to various environmental influences that can lead to degradation of the insulating material. Accordingly, these materials must meet various minimum requirements with regard to their properties (e.g., UV resistance) [2]. Especially in outdoor applications and under severe indoor conditions, contamination layers may be deposited on the surface, which contains electrically conductive particles (e.g., salts). If the material does not exhibit hydrophobic properties or has temporarily lost them, a conductive pollution layer can be formed by the presence of moisture. As a result, electrical surface discharges, so-called dry band discharges or high voltage arcs, can occur. The insulating materials used under these conditions must have sufficient resistance to such discharges. This is verified for AC applications by means of various test methods (e.g., inclined plane test according to IEC 60587 [3], high-voltage arc test according to IEC 61621 [4]).

Tests of the tracking and erosion resistance with DC voltage usually show both considerably greater damage and a greater scatter of results [5]. It is assumed this is caused by a higher local and temporal stability of the discharges as well as a higher power transfer [6], [7]. The

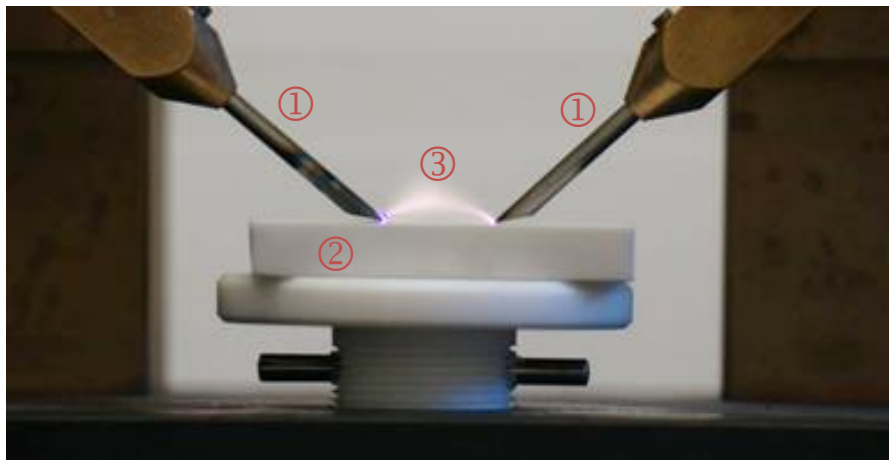
thermal effect of low-current surface discharges is considered to be the main effect of damage or decomposition of polymer insulating materials. [8], [9], [10].

Based on this assumption, a thermal model is developed to calculate the heating of insulating material surfaces by electrical surface discharges. This model should allow conclusions on the thermal stress of insulating material surfaces and support the interpretation of measurement results, especially on the influence of the voltage type. Furthermore, the evaluation of different influencing factors on the heating (thermal conductivity of the insulating material) should be made possible and e.g., a specific material optimization for DC voltage applications should be facilitated. The knowledge gained on the basis of the model also flows into the development of a test procedure for evaluating the DC erosion and tracking resistance.

In the first step, a model is used for an AC arc and a geometrically simplified electrode arrangement with an inert insulating material. In the future, the model will be extended to include more complex geometries, insulation decomposition, DC stress, and sensitivity studies will be performed.

1 Model Test Setup and Temperature Measurements

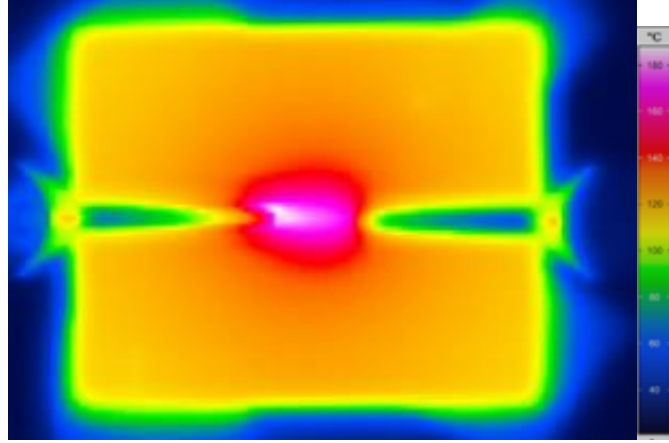
As a simple geometric experimental arrangement, the electrode arrangement of the high voltage arc test according IEC 61621 [4] is used, as shown in Fig. 1. A low-voltage arc (3) is ignited between two tungsten electrodes (1). The heat of the hot plasma is transferred to the surface of the ceramic test specimen (2) by heat radiation, convection and conduction. Convection is the dominant effect [11]. For the heat distribution in the test specimen, heat conduction is the predominant effect mechanism.



Source: Own

Fig. 1: Electrode arrangement according IEC 61621: (1) tungsten electrode; (2) ceramic specimen; (3) high voltage arc

The test voltage of 12.5 kV (rms value) is generated by a high voltage transformer (max. 17 kV, 4.4 kVA). The test circuit is conforming with IEC 61621. The arc current is adjusted by a variable series resistor on the primary side of the transformer. The current is measured by a shunt resistor and recorded by A/D converter. The arc voltage is measured by an ohmic voltage divider and recorded as well. To avoid influences of the arc by the thermal decomposition of the test specimen, an inert test specimen made of aluminum oxide ceramic (Al_2O_3) with the dimensions 38 mm x 33 mm x 6 mm is used for these experiments. The heating of the test specimen is recorded with a thermal imaging camera “VarioCAM hr head” from InfraTec GmbH and recorded with a measuring frequency of 1 Hz (Fig. 2). The camera is placed at an angle of 90° above the test specimen. The arc is applied to the specimen for 60 minutes overall with continuous temperature measurement.



Source: Own

Fig. 2: Example of a thermogram (20 mA, 500 s)

At the given geometrical set-up one pixel of the IR camera corresponds to a square of about 0.4 mm of the specimen. The pixels are combined in such a way that they correspond to the size of the nodes of the calculation model. Parameters of the temperature measurement are summarized in Tab. 1.

Tab. 1: Parameters of the temperature measurement

Distance to IR camera	48 cm
Angle to surface	90°
Instantaneous Field of View (IFOV)	0.8 mrad
measurement spot size	0.38 mm
Measurement frequency	1 Hz
Emissivity Al_2O_3	0.9

Source: Own

2 Modeling of the Dynamic Behavior of the Surface Temperature for the Experimental Setup

The thermal model of the above-mentioned experimental setup consists of three sub-models that mathematically describe different physical mechanisms. Sub-model 1 describes the arc as a current-voltage model (VCM), the 3-cylinder model (3CM) determines the heat fluxes from the arc to the specimen surface (sub-model 2), and the third (THM) determines the resulting surface temperature due to heat transport within the specimen and to the environment.

The overall model serves the purpose of investigating the influence of the various parameters and their uncertainties on the result.

The sub-models are described in detail in the following sections.

2.1 Sub-Model 1: Arc as Voltage-Current Model (VCM)

If a 50 Hz alternating voltage is applied to the described electrodes it leads to periodical electrical stress to the air gap. If the voltage exceeds the electrical strength of the air a break-through will occur and an electrical discharge is created. The gas is ionized and forms plasma that can reach extremely high temperatures, depending on the carried current. The conditions used in these experiments result in a discharge called a high voltage arc. Using alternating voltage, this process essentially occurs with every change from positive to negative half-wave. If the voltage exceeds a certain amount, the arc ignites. This voltage is defined as ignition voltage U_{it} , whereby the moment this occurs is called ignition moment t_I . If the

voltage falls below the minimum required for the arc, the extinction voltage U_{t2} , the arc extinguishes. This moment is defined as extinction moment t_2 .

The equations are documented in detail in [10]. The characteristic values were determined from the measurement results of the performed experiments. The voltage and current of the arc are described by equations (1) and (2). The sign function “*sign*” is used to take care of the positive and negative half-wave:

$$u_a(t) = \sqrt{2} \cdot U_a \cdot \sin(\omega_u \cdot t) \cdot \frac{1 + \text{sign}((t-t_1)(t-t_2))}{2} + \left[U_{t1} - \frac{U_{t1} - U_{t2}}{t_2 - t_1} \right] \cdot \frac{1 - \text{sign}((t-t_1)(t-t_2))}{2} \quad (1)$$

$$i_a(t) = \sqrt{2} \cdot I_a \cdot \sin\left(\omega_i \cdot \left(t - \left(\frac{\pi}{\omega_u} - t_2\right)\right)\right) \cdot \frac{1 - \text{sign}((t-t_1)(t-t_2))}{2} \quad (2)$$

In the model, interpolation with a 7th-order polynomial is used to describe the part when the arc is ignited. Tab. 2: summarizes the experimentally determined parameters, exemplarily for a test current of 40 mA.

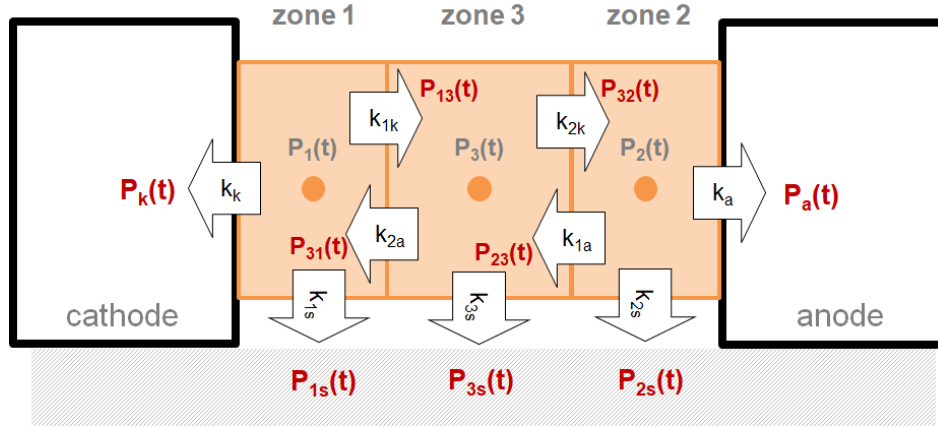
Tab. 2: Parameters for arc current-voltage model using the example of test current 40 mA

Parameter	Value	Description
U_a / kV	13	RMS value of the voltage
I_a / mA	40	RMS value of current
U_{t1} / kV	2.1	Ignition voltage
U_{t2} / kV	1.297	Extinguishing voltage
ω_u / rad / ms	0.314	Circular frequency of the voltage
ω_i / rad / ms	0.314	angular frequency of the current
t_1 / ms	0.402	Ignition moment
t_2 / ms	9.68	Extinguishing moment

Source: Own, inspired by [10]

2.2 Sub-Model 2: Arc as 3-Cylinder Model (3CM)

The 3-cylinder model determines the heat flows that warm the test specimen. The model represents the arc as a straight cylinder. This is divided into three cylinders (zones 1-3), see Fig. 3. The electrical power within the arc forms the basis for the heat flows to the test specimen. The electrical power is allocated in equal parts to the three cylinders (zones) as $P_1(t)$, $P_2(t)$ and $P_3(t)$. The respective k-factors determine the weighting of the individual heat flows within the arc ($P_{13}(t)$, $P_{32}(t)$, $P_{31}(t)$, $P_{23}(t)$) as well as those flowing to the electrodes ($P_k(t)$, $P_a(t)$) and the specimen ($P_{1s}(t)$, $P_{2s}(t)$, $P_{3s}(t)$). The physical meaning of the k-factors is explained in [12] and the values are adapted from [10], cf. Tab. 3.



Source: Own, based on [10]

Fig. 3: Resulting heat flows to the test specimens and the zoning of the 3-cylinder model according to [12]

The parameters from Fig. 3: have the following meaning:

- $P_k(t)$ – heat flux delivered to the cathode,
- $P_a(t)$ – heat flux delivered to the anode,
- $P_{1s}(t)$, $P_{2s}(t)$, $P_{3s}(t)$ – thermal power transferred from the respective zone to the material surface.
- the corresponding k -factors have indices that characterize their source and sink:
 - a – the anode,
 - k – cathode respectively,
 - s – material surface.

As shown in Fig. 3, five heat fluxes result from the arc affecting the specimen and the electrodes. The heat flows from the arc to the rest of the environment are not explicitly calculated. The heat dissipation over the shell surface is primarily weighted by the factors k_{1s} , k_{2s} and k_{3s} . The value of 0.33 defines a heat dissipation of one third of the shell surface to the test specimen. The remaining two thirds of the heat are transferred to the environment. Equations (3), (4) and (5) describe, exemplarily, the calculation of the heat flow $P_k(t)$, which is transferred through the circular surface of the arc cylinder (front surface of the arc at the cathode) via the cathode to the test specimen surface. The parameters are summarized in Tab. 3.

The heat flow to the cathode $P_k(t)$ is composed as follows [10], [12]:

- Heat flow from zone 2 to zone 3:

$$P_{23}(t) = \frac{1}{2}k_{1a} \cdot P_2(t) \cdot \left(1 - \frac{d_2(t)}{\sqrt{a_2(t)^2 + d_2(t)^2}}\right) \quad (3)$$

- Heat flow from zone 3 (incl. zone 2) to zone 1:

$$P_{31}(t) = k_{2a} \cdot \left(P_{23}(t) + \frac{1}{2}P_3(t) \cdot \left(1 - \frac{d_3(t)}{\sqrt{a_3(t)^2 + d_3(t)^2}}\right)\right) \quad (4)$$

- The resulting heat flow from zone 1 (incl. zone 2 + 3) via cathode to test specimen:

$$P_k(t) = \frac{1}{2}k_k \cdot \left(P_{31}(t) + P_1(t) \cdot \left(1 - \frac{d_1(t)}{\sqrt{a_1(t)^2 + d_1(t)^2}}\right)\right) \quad (5)$$

The model was developed for arcs with significantly larger current values [12]. It is being investigated whether the model can also be used for low currents (10 mA - 40 mA) [10].

Tab. 3: Parameters for the 3-cylinder model

Parameter	Value	Description
d_1, d_2 [mm]	1	Half cylinder length zone 1 (cathode) and zone 2 (anode)
d_3 [mm]	2.5	Half the cylinder length of zone 3 (arc column)
a_1, a_2, a_3 [mm]	$k_L \cdot i_a(t)$	Radii of the cylinders (product of current $i_a(t)$ and proportionality factor k_L)
k_{1a} [-]	0.2	Weighting coefficient of heat flow from zone 2 to zone 3
k_{2a} [-]	0.2	Weighting coefficient of heat flow from zone 3 to zone 1
k_a [-]	0.3	Weighting coefficient of heat flow from zone 2 to anode
k_{1k} [-]	0.2	Weighting coefficient of heat flow from zone 3 to zone 1
k_{2k} [-]	0.5	Weighting coefficient of heat flow from zone 3 to zone 2
k_k [-]	0.3	Weighting coefficient of heat flow from zone 2 to cathode
k_{1s} [-]	0.33	Weighting coefficient of the heat flux from zone 2 to the test specimen surface
k_{2s} [-]	0.33	Weighting coefficient of the heat flux from zone 2 to the test specimen surface
k_{3s} [-]	0.33	Weighting coefficient of the heat flux from zone 2 to the test specimen surface
k_L [mm / mA]	0.0065	Proportional factor arc diameter to current
L_a [cm]	0.7	arc length

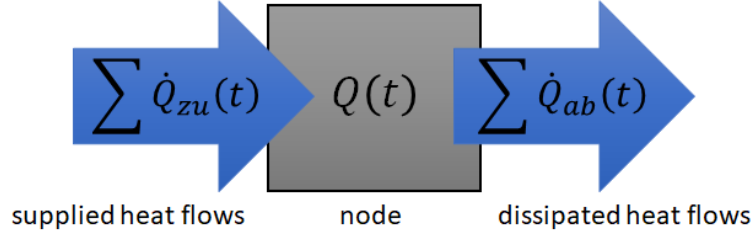
Source: Own, inspired by [10], [12]

Considering the duration of about 1 h until a steady-state surface temperature is established. It makes sense to choose the simulation step size as large as possible. The dynamics of the temperature model is significantly lower than that of the arc as voltage-current model (VCM). The time constants are between 0.01 s and 0.1 s and the period of the sinusoidal oscillation is 20 ms (50 Hz). With a recommended simulation step size of one-tenth of the period duration (Shannon sampling theorem) [13], this results in a constant step size of 0.002 s. This leads to an enormous computational effort (computing time). For this reason, the RMS values of arc current, arc voltage, arc power, and the resulting heat flows are used for further simulations. The investigations show that there are no significant differences in the resulting surface temperature curves compared to the use of the time curves of current, voltage, and power. By using the RMS values, it is possible to perform the simulations with a variable step size depending on the dynamics of the temperature model. This leads to the next chapter of the arc as a temperature-heat model (THM).

2.3 Sub-Model 3: Temperature-Heat Model (THM)

The third sub-model determines the surface temperature of the test specimen from the resulting heat flows. The physical basis is the heat transport within the test specimen and to the environment. Specifically, the mechanisms of convection and heat conduction are considered. Heat radiation from the test specimen to the environment is neglected due to its minor influence [11].

Heat balancing was chosen as the modeling approach. The principle is shown in Fig. 4 and results in differential equation (6). The heat $Q(t)$ for a volume element (node) is considered. The temporal change of this heat depends on the temporally supplied $\dot{Q}_{zu}(t)$ and dissipated heat flows $\dot{Q}_{ab}(t)$.



Source: Own

Fig. 4: Model idea of the heat balancing

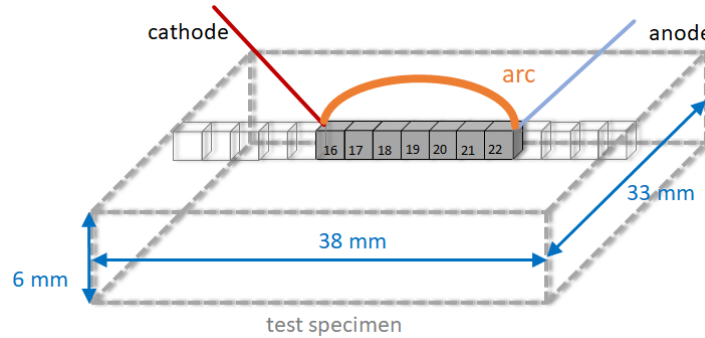
$$\frac{dQ(t)}{dt} = \sum \dot{Q}_{zu}(t) - \sum \dot{Q}_{ab}(t) \quad (6)$$

The specimen is divided into 38 nodes along the arc, as illustrated in Fig. 5. A node has the dimension of 0.001 m x 0.0033 m x 0.0006 m (length x width x height). The remaining test specimen is considered as one large node. For each node, a differential equation is set up, i.e., for 39 nodes, a differential equation system results, which consists of 39 differential equations.

The time-dependent heat $Q(t)$ of a node is described by equation (7).

$$Q(t) = m_{Node} \cdot c_{pNode} \cdot \vartheta_{Node}(t) \quad (7)$$

Equation (7) is the product of the material mass of the node m_{Node} , the heat capacity c_{pNode} and the temperature of the nodes $\vartheta_{Node}(t)$. The mass and heat capacity are considered constant.



Source: Own

Fig. 5: Scheme of the node arrangement, arc and test specimen

In addition to the energy supplied by the arc, the test specimen (between the nodes) is affected by thermal conduction and through the test specimen surface by thermal convection (heat dissipation to the environment). The thermal conductivity $\dot{Q}_{Leit}(t)$ in a homogeneous material is generally defined by equation (8) [14]

$$\dot{Q}_{Leit}(t) = \lambda(t) \cdot A \cdot \left(\frac{d\vartheta_x(t)}{dx} \right)_x \quad (8)$$

where $\lambda(t)$ describes the thermal conductivity of the test specimen material. This is temperature dependent. A is the area to the neighboring node and $d\vartheta_x(t)/dx$ describes the temporal change of the temperature along one dimension (x -axis). By referring to two adjacent nodes, equation (8) becomes equation (9)

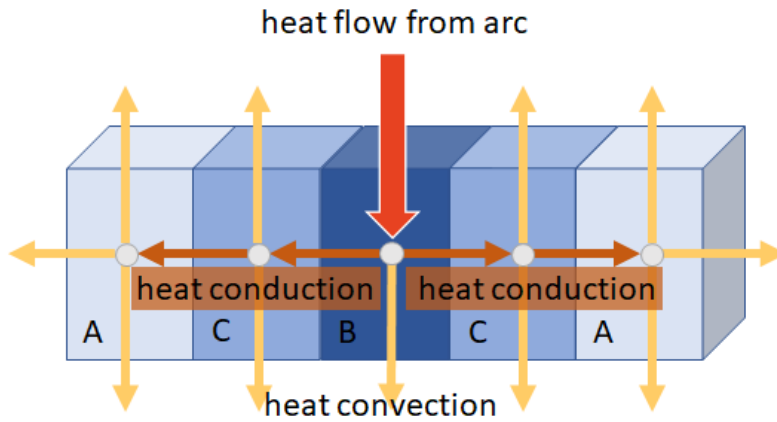
$$\dot{Q}_{Leit}(t) = \lambda(t) \cdot A \cdot \left(\frac{\vartheta_{Nb}(t) - \vartheta_{Node}(t)}{\Delta x} \right)_x \quad (9)$$

where $\vartheta_{Nb}(t)$ stands for the temperature of the neighboring node. The distance of the node centers is defined by Δx . The heat convection $\dot{Q}_{konv}(t)$ to the environment is determined by equation (10). The heat transfer coefficient α describes the intensity of heat transfer at the specimen surface and A_O is the surface over which the heat flux flows to the environment [14].

$$\dot{Q}_{konv}(t) = \alpha \cdot A_O \cdot (\vartheta_{Node}(t) - \vartheta_U) \quad (10)$$

With equations (6), (7), (9) and (10) plus a part of the heat flow from the arc, the respective differential equations for the nodes are set up. Three different basic equations crystallize, which differ in the heat fluxes supplied and dissipated. Fig. 6 illustrates the three different types:

- Type A: These are the two nodes on the left and right edges of the specimen. The heat flow supplied is defined by the heat conduction from the neighboring node. Heat is dissipated by convection to the environment and by conduction to the rest of the specimen.
- Type B: Is characterized by the heat supply of the arc. The heat is dissipated to the cooler neighboring nodes by heat conduction. These nodes are located under the arc.
- Type C: These nodes are located between the edge nodes and the under the arc nodes. They absorb heat by conduction from the warmer neighbor and transfer it to the cooler one as well as to the rest of the specimen. Heat is transferred to the environment via the surface by convection.



Source: Own

Fig. 6: Scheme of model representation for the different node types based on the resulting heat balances.

As an example, the resulting differential equation (11) for type B (nodes under the arc) is given. $\dot{Q}_{LB}(t)$ represents the heat flux from the arc. Equation (11) describes how the temperature of the node $\vartheta_B(t)$ changes in time as a function of the heat fluxes supplied and removed.

$$\begin{aligned} & \frac{m_B \cdot c_{p_B}}{G_B} \cdot \frac{d\vartheta_B(t)}{dt} + \vartheta_B(t) = \\ & = \frac{1}{G_B} \cdot \dot{Q}_{LB}(t) + \frac{\alpha_B \cdot A_{OB}}{G_B} \cdot \vartheta_U + \frac{\lambda_{Pr} \cdot A_{lr}}{\Delta x \cdot G_B} \cdot \vartheta_l(t) + \frac{\lambda_{Pr} \cdot A_{lr}}{\Delta x \cdot G_B} \cdot \vartheta_r(t) + \frac{2 \cdot \lambda_{Pr} \cdot A_{Pr}}{h \cdot G_B} \cdot \vartheta_{Pr}(t) \end{aligned} \quad (11)$$

where

$$G_B = \frac{\alpha_B \cdot A_{OB} \cdot \Delta x \cdot h + 2 \cdot \lambda_{Pr} \cdot A_{Ir} \cdot h + 2 \cdot \lambda_{Pr} \cdot A_{Pr} \cdot \Delta x}{\Delta x \cdot h} \quad (12)$$

Tab. 4: contains the explanations of the parameters used. The differential equation system is composed of 39 DGL (two type A, seven type B, and 29 type C). For the first studies, it is assumed that the material parameters (thermal conductivity, heat capacity, density, heat transfer coefficient) are independent of temperature.

Tab. 4: Parameters used in equations (11) and (12)

Parameter	Explanation
Dx	Distance of the node centers (symmetrical)
h	Node height
A_{Ir}	Surface to neighboring node (left and right neighbor)
A_{Pr}	Surface between node and remaining test specimen
A_{OB}	Surface between node and environment
m_B	Mass of a node (density [3800 kg / m ³])
l_{Pr}	Thermal conductivity of the test specimen material
c_{pB}	Heat capacity of the test specimen material [950 W / (kg * K)]
a_B	Heat transfer coefficient [12 W / (m * K)]
$\vartheta_B(t)$	Node temperature
$\vartheta_l(t)$	Temperature of the left neighboring node
$\vartheta_r(t)$	Temperature of the right neighbor node
$\vartheta_{Pr}(t)$	average temperature of the remaining test specimen
ϑ_U	Environmental temperature [295 K]

Source: Own

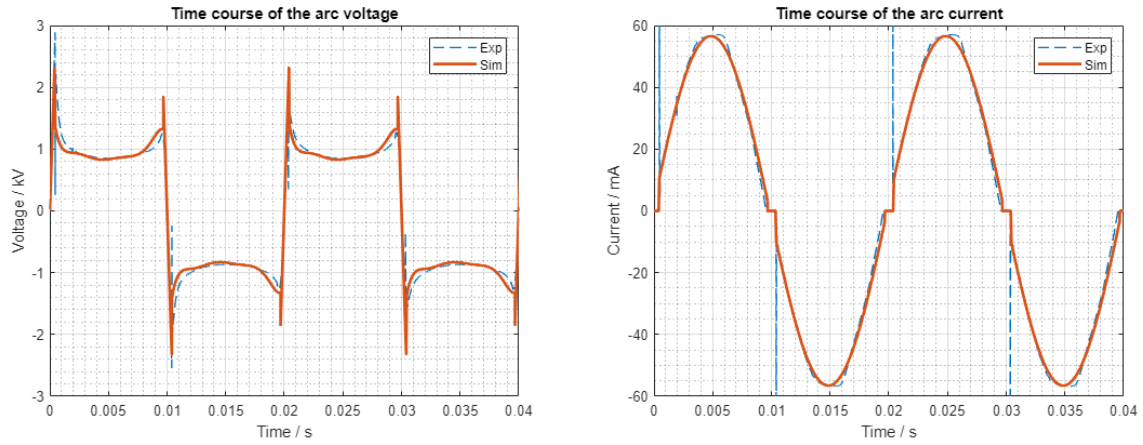
3 Verification and Validation of the Model

The simulations of the temporal behavior are carried out with MATLAB[®]. The aim is to determine the change in surface temperature over time for different test current levels (10, 20, 30 and 40 mA) and to validate the models using the measured data.

The general model behavior is plausible, with increasing current intensity the surface temperature increases. The surface temperature also reaches a stable steady-state final value. Like mentioned above the model behavior are investigated with the time characteristics of current and voltage and the RMS values. No difference in the resulting surface temperatures was observed.

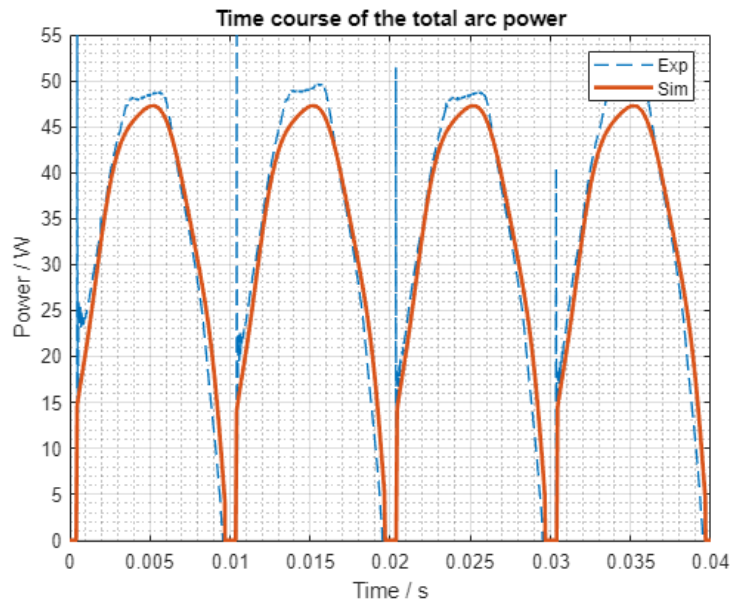
3.1 Validation of Sub-Model 1: Voltage-Current Model (VCM)

As an example, the validation is carried out with a test current of 40 mA. The curve of the arc voltage is shown in Fig. 7 (left) and of the arc current in Fig. 7 (right). Two periods were shown (40 ms). The blue curves are the experimentally obtained data and the orange curves are the calculated time curves. Fig. 8 shows the curve of the electric arc power. The achieved agreement is qualitatively and quantitatively very good.



Source: Own

Fig. 7: Time course of the arc voltage (left) and time course of the leakage current in the arc (right) for a test current of 40 mA: blue – experimental data; orange – simulation data



Source: Own

Fig. 8: Time course of the arc power for a test current of 40 mA: blue – experimental data; orange – simulation data

When comparing the RMS values of the arc voltage and arc current, cf. Tab. 5, a relative error of approx. 3% is found for the voltage and 1% for the current.

Tab. 5: Comparison of the rms values of the arc voltage and arc current

Data source	Arc voltage [kV]	Arc current [mA]	Relative arc voltage [%]	Relative arc current [%]
Experimental data	1.03	40.4	100	100
Model data	0.996	39.97	97	99

Source: Own

3.2 Validation of Sub-Model 2: 3-Cylinder Model (3CM)

To validate the model, heating calculations were first performed with a test current of 10 mA and compared with the measured data. The electrical power of the high-voltage arc is equally distributed for all three cylinder elements (cathode, column and anode), as described in section 2.2. Tab. 6 contains the experimental and calculated data.

Tab. 6: Data on the distribution of electrical power in the high-voltage arc

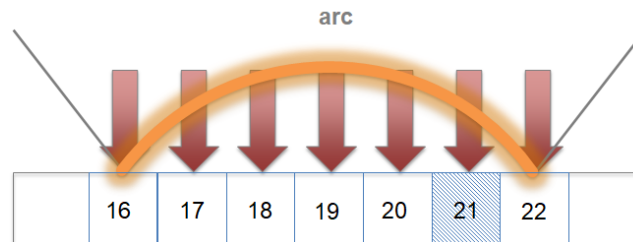
Test current	Data source	Electrical power / W			
		Total	Cathode	Plasma	Anode
10 mA	Experiment	12.1	4.03	4.03	4.03
	Model	12.6	4.20	4.20	4.20
20 mA	Experiment	20.4	6.80	6.80	6.80
	Model	20.9	9.96	6.98	9.96
30 mA	Experiment	29.5	9.83	9.84	9.83
	Model	28.8	9.60	9.60	9.60
40 mA	Experiment	36.2	12.13	12.13	12.13
	Model	35.4	11.80	11.80	11.80

Source: Own

The total power determined from the measured values was used as the output variable. The electrical power at the cathode and anode was calculated from the corresponding voltage drops of the literature. The column voltage was determined from the difference between the total power and the power at the anode and cathode.

3.3 Validation of Sub-Model 3: Temperature-Heat Model (THM)

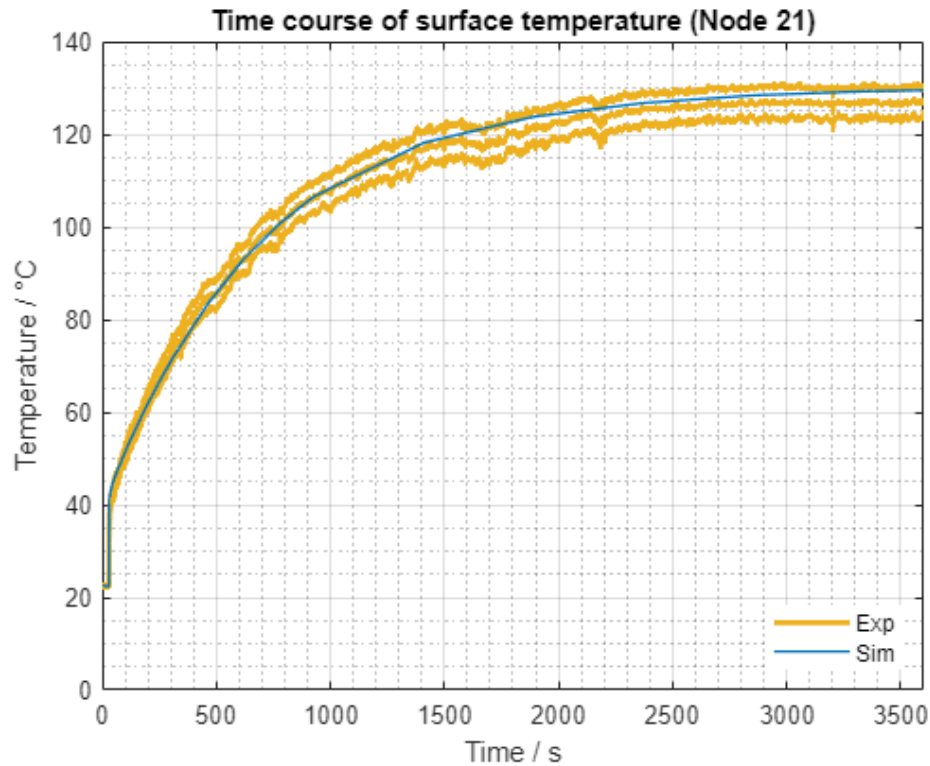
Fig. 9 illustrates the node distribution under the arc.



Source: Own

Fig. 9: Scheme of the node distribution below the arc

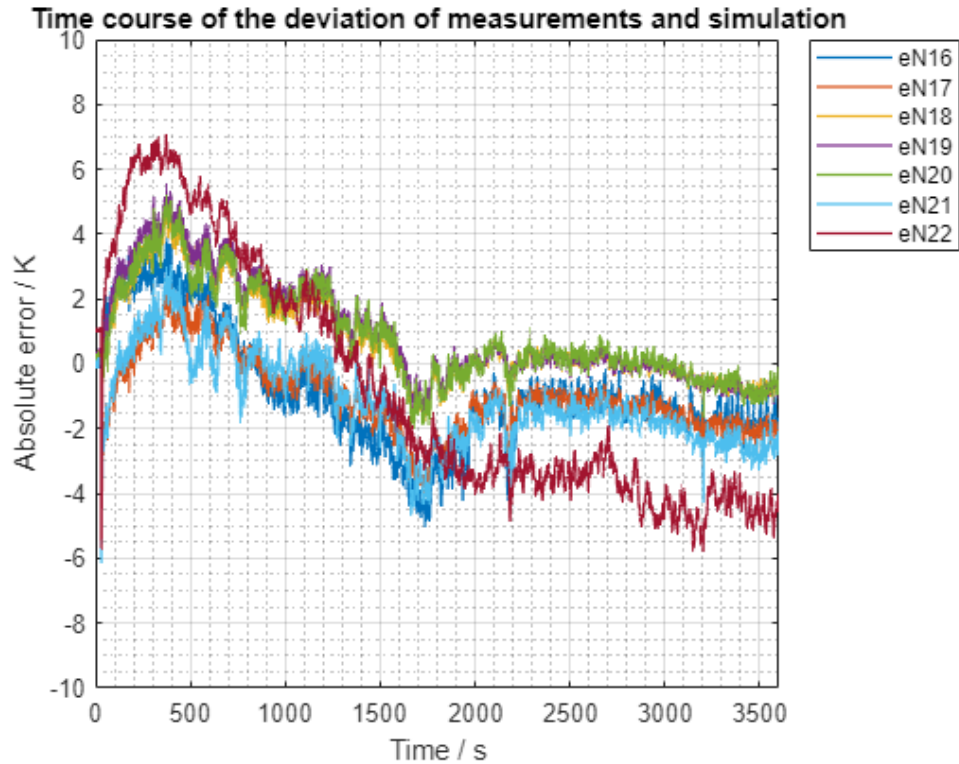
Fig. 10 shows an example of the time curve of the surface temperature in node 21 between the mean value of the experiments and the simulation for an alternating test current of 10 mA. At a time of 30 s, the arc is ignited and there is a very steep rise in the surface temperature. The increase decreases and becomes approximately linear after 40 s. The simulation results mirror the measured values. This shows that the results are within the confidence interval of the averaged values of the tests.



Source: Own

Fig. 10: Time course of the surface temperature in Node 21 between the mean value of the experiments (with the confidence interval of 95%) and the simulation for a test current of 10 mA

This becomes clearer in Fig. 11, which shows the deviation over time between the mean value of the experiments and the simulation for all nodes under the arc. The chart shows that the deviations for the nodes at the edge (nodes 16 and 22) are greater than for those in the middle. The largest deviation is about 5 K.



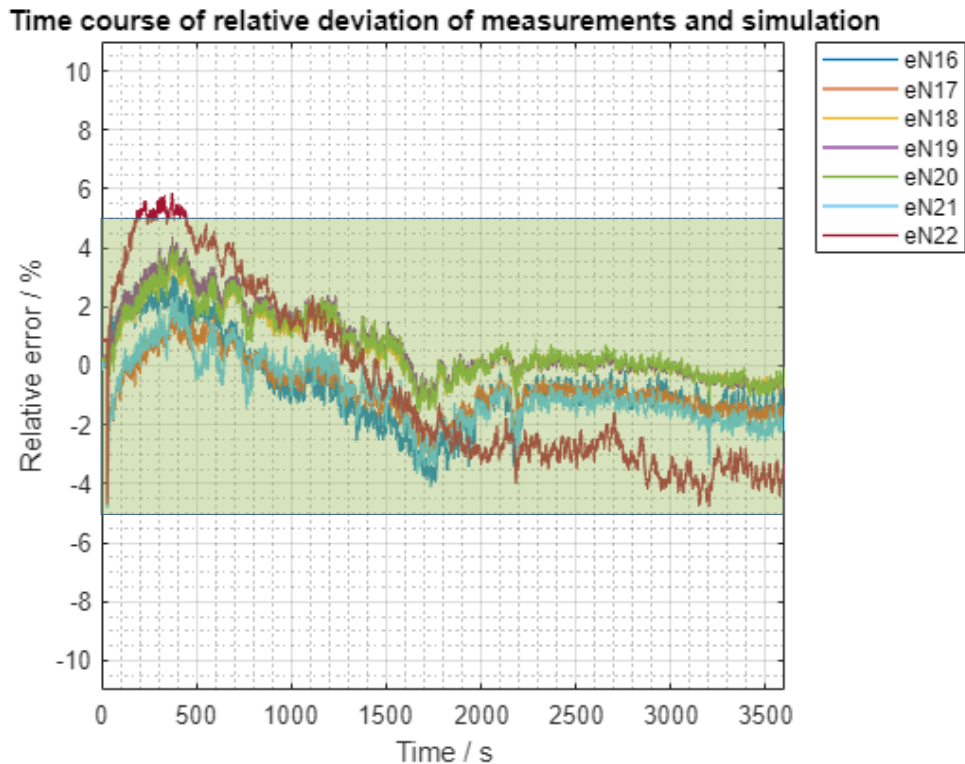
Source: Own

Fig. 11: Time course of the deviation between the mean value of the experiments and the simulation for all nodes under the arc for a test current of 10 mA

Analyzing the relative error, shown in Fig. 12, it is clear that the error for the middle nodes (17-21) is in an error band of $\pm 2\%$. In general, the relative error is smaller than $\pm 5\%$ (green zone). This allows the conclusion that the model reflects the experiments very well and it is suitable for the given experimental constellation to be used as a prediction tool.

In order to minimize the errors, the following improvements are to be investigated in further work. In the next step, the temperature dependence of the material values density, thermal conductivity, heat capacity, and the heat transfer coefficient will be investigated. A further increase of the model accuracy is the increase in the number of nodes.

Finally, the model seems to be suitable to determine the thermal stress caused by electrical surface discharges.



Source: Own

Fig. 12: Time course of the relative deviation between the mean value of the experiments and the simulation for all nodes under the arc for a test current of 10 mA

Conclusion

In this article a thermal model is presented which describes the heating of insulation surfaces by low current discharges. The model consists of three parts describing the electrical and thermal characteristic of the arc as well as of heat dissipation to and in the specimen. The model output is compared with experimental data of measurements of the arc voltage and current. Further temperature measurements of with an IR camera are used to verify the model.

The combination of the three sub-models is in very good accordance with the experimental data regarding absolute values and dynamic response. The model was successfully verified and validated. It is concluded that the models are basically applicable to describe the heating of surfaces by low current arcs.

This model will be the base for further investigations and a modification to describe the heating in the case of a DC arc. In a further step, the various influences of the parameters on the surface temperature are explored, and how uncertainties affect the determination of the parameters. A further extension of the model is considered to examine e.g., the effect of material degradation or combustion on the surface heating.

Acknowledgments

The authors would like to acknowledge Hochschule Zittau/Görlitz, University of Applied Sciences for their support of this research.

Literature

- [1] PAPAILIOU, K. O.; SCHMUCK F.: *Silikon-Verbundisolatoren – Werkstoffe, Dimensionierung, Anwendungen*. Springer Verlag, Berlin, 2011. ISBN 978-3642238130.
- [2] IEC TR 62039 – *Selection guide for polymeric materials for outdoor use under HV stress*. 2007.
- [3] IEC 60587:2007 – *Electrical insulating materials used under severe ambient conditions - Test methods for evaluating resistance to tracking and erosion*. 2007.
- [4] IEC 61621 – *Dry, solid insulating materials – Resistance test to high-voltage, low-current arc discharges*. 1997.
- [5] CIGRÉ WORKING GROUP D1.27: *Feasibility Study for a DC Tracking and Erosion Test*. Technical brochure 611. 2015.
- [6] KUEHNEL, S.; KORNUBER, S.; LAMBRECHT, J.: On the Electrical Characteristic and Heat Dissipation of High Voltage Surface Arcs. *IEEE Conference on Electrical Insulation and Dielectric Phenomena (CEIDP)*. Cancun, Mexico, 2018. DOI: [10.1109/CEIDP.2018.8544746](https://doi.org/10.1109/CEIDP.2018.8544746)
- [7] CERVINKA, R.; BÄRSCH, R.; SEIFERT, J.: Einfluss der Prüfspannungsart auf das Oberflächenverhalten von polymeren Isolierstoffen unter elektrolytischen Fremdschichtbelastungen. *ETG-Fachbericht*. Vol. 125, pp. 69–75. VDE-Verlag Berlin-Offenbach, 2010.
- [8] MENZEL, W.: *Zur Klimabeständigkeit von Kunststoff-Innenraumisolierungen mit Oberflächenbeschichtungen*. Dissertation, Technische Hochschule Zittau, 1989.
- [9] EL-HAG, A.; MEYER, L. H.; NADERIAN, A.: Experience with Salt-Fog and Inclined-Plane Tests for Aging Polymeric Insulators and Materials. *IEEE Electrical Insulation Magazine*. 2010, Vol. 26, Issue 2, pp. 42–50. DOI: [10.1109/MEI.2010.5482554](https://doi.org/10.1109/MEI.2010.5482554)
- [10] ZHANG, X.; ROWLAND, S. M.: Modelling of dry-band discharge events on insulation surfaces. *IEEE International Symposium on Electrical Insulation*. San Diego, CA, USA, 2010. DOI: [10.1109/ELINSL.2010.5549489](https://doi.org/10.1109/ELINSL.2010.5549489)
- [11] KIM, S.-H.; HACKAM, R.: Temperature distribution in RTV silicone rubber coating following band arcing. *Proceedings of 1994 IEEE International Symposium on Electrical Insulation*. Pittsburgh, PA, USA, 1994. DOI: [10.1109/ELINSL.1994.401383](https://doi.org/10.1109/ELINSL.1994.401383)
- [12] BORKOWSKI, P.; WALCZUK, E.: Thermal Models of Short Arc between High Current Contacts. *Proceedings of the Forth-Seventh IEEE Holm Conference on Electrical Contacts (IEEE Cat. No.01CH37192)*. Montreal, QC, Canada, 2001. DOI: [10.1109/HOLM.2001.953220](https://doi.org/10.1109/HOLM.2001.953220)
- [13] KAHLERT, J.: *Simulation technischer Systeme*. Friedr. Vieweg & Sohn Verlag / GWV Fachverlage GmbH, Wiesbaden, 2004. ISBN 978-3-322-80248-4. eBook ISBN 978-3-322-80247-7. DOI: [10.1007/978-3-322-80247-7](https://doi.org/10.1007/978-3-322-80247-7)
- [14] VDI e. V.: *VDI-Wärmeatlas*. Springer Vieweg Berlin, Heidelberg, 2013. Series ISSN 2512-5281. Series E-ISSN 2512-529X. DOI: [10.1007/978-3-642-19981-3](https://doi.org/10.1007/978-3-642-19981-3)

Dipl.-Ing. (FH) Daniel Fiß; Dipl.-Ing. (FH) Stefan Kühnel; Ernest Krzyszkowski;
prof. Dr. techn. Stefan Kornhuber

MODELOVÁNÍ ČASOVÉHO CHOVÁNÍ POVRCHOVÉ TEPLOTY POVRCHU IZOLAČNÍHO MATERIÁLU PŘI NÍZKOPROUDÉM OBLOUKU

V tomto článku je představen výpočetní model, který lze použít k předpovědi ohřevu povrchů izolačních materiálů nízkoproudými vysokonapěťovými oblouky. Výboj je reprezentován tzv. tříválcovým modelem. Na jeho základě jsou vypočteny tepelné toky na povrchu izolačního materiálu a jeho ohřev pomocí tepelné kondukce a konvekce. Výsledky výpočtu jsou porovnány s měřením povrchové teploty na modelovém uspořádání. Celkový model velmi dobře reprodukuje dynamické chování ohřevu. Kvantitativní odchylky od měření se pohybují pouze v řádu několika procent.

MODELLIERUNG DES ZEITLICHEN VERHALTENS DER OBERFLÄCHENTEMPERATUR EINER ISOLIERSTOFFOBERFLÄCHE UNTER EINEM STROMSCHWACHEN LICHTBOGEN

In vorliegenden Beitrag wird ein Berechnungsmodell vorgestellt, mit welchem die Erwärmung von Isolierstoffoberflächen durch stromschwache Hochspannungs-Lichtbögen vorausberechnet werden kann. Die Entladung wird dabei durch ein sog. Drei-Zylinder-Modell abgebildet. Ausgehend davon werden die Wärmeströme auf die Isolierstoffoberfläche und deren Erwärmung mittels Wärmeleitung und Konvektion berechnet. Die Berechnungsergebnisse werden mit Messungen der Oberflächentemperatur an einer Modellanordnung vergleichend bewertet. Das Modell bildet das dynamische Verhalten der Erwärmung sehr gut ab. Die quantitativen Abweichungen zur Messung liegen lediglich im Bereich weniger Prozente.

MODELOWANIE CZASOWEGO ZACHOWANIA SIĘ TEMPERATURY POWIERZCHNI MATERIAŁU IZOLACYJNEGO POD WPLYWEM ŁUKU ELEKTRYCZNEGO O NISKIM NATĘŻENIU PRĄDU

W niniejszym opracowaniu przedstawiono model obliczeniowy, który może być stosowany do prognozowania nagrzewania powierzchni materiałów izolacyjnych przez wysokonapięciowe łuki o niskim natężeniu prądu. Wyładowanie jest reprezentowane przez tzw. model trzycylindrowy. Na jego podstawie oblicza się przepływy ciepła na powierzchnię materiału izolacyjnego oraz jego nagrzewanie przy pomocy kondukcji ciepła i konwekcji. Wyniki obliczeń porównane są z pomiarami temperatury powierzchni na układzie modelowym. Cały model bardzo dobrze odtwarza dynamiczne zachowanie ogrzewania. Ilościowe odchylenia od pomiarów są rzędu kilku procent.

INNOVATION OF ELECTRONIC CONTROL OF THE AIR FOR THE FIREPLACE STOVE

Josef Hykl

Technical University of Liberec, Faculty of Mechanical Engineering,
Department of the Design of Machine Elements and Mechanisms,
Studentská 2, 416 17, Liberec 1, Czech Republic
e-mail: josef.hykl@tul.cz

Abstract

The electronic air damper is a system used for automated control of air distribution in fireplaces without human intervention. It is designed to meet specified criteria, such as primary and secondary air distribution, environmental friendliness (design of environment), and easy replacement and services of functional parts (design of service). Conventional fireplace stoves can be regulated with primary and secondary air, which are controlled manually or in combination with an automatic damper. The average user is not able to tune the ratio of primary and secondary air in the ratio that has been tested in an official testing laboratory. Moreover, the average user is usually not even familiar with the terms secondary and primary air. It is necessary to innovate the air control system.

Keywords

Fireplace stove; Combustion chamber; Throttle valve; Air dumper; Automatization.

Introduction

Laziness is the mother of progress. In today's automated world, about 40% [1] of the population still heats with wood stoves in their homes. Designers keep the comfort of these users in mind and take progress into account when developing automated stove control. The electronic damper for automated air distribution control is largely in line with this idea. Another factor that plays an important role in electronic control is meeting future international standards for the sustainability of the planet. It is common knowledge that users of fireplace stoves often use them at their own discretion and not always in an entirely optimal and correct way. Controlling the air flowing into the stove is one of the key factors in wood heating when it comes to combating the impact of harmful emissions on the environment. More than 160 countries around the world [2] have formulated their environmental strategy.

The world is moving forward, towards environmental protection. Electronic air control in the fireplace stove is only one fragment. However, the individual fragments form the overall mosaic of the sustainability of the planet.

1 Materials and Methods

1.1 Theory

Figure 1 shows the historical development from antiquity with open fireplaces to the present. The middle picture shows a product called *Petry*, which was very popular in Czechoslovakia in the 1980s. But the development does not stop there. In the picture on the right there is a modern fireplace stove.



Source: Own

Fig. 1: Historical development

There are many different kinds of fireplace stoves in the world (Fig. 2).



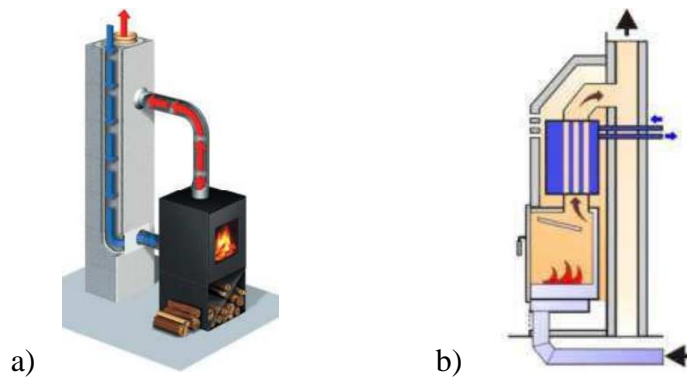
Source: Database of the ABX, spol. s r. o.

Fig. 2: Morphology of fireplace stoves

However, all types have two things in common: good combustion and clean glass.

The combustion process must be controlled. The aim of the controlled combustion process is to get as close as possible to perfect combustion. Since it is technically impossible to achieve this state in an ordinary stove, a larger amount of combustion air must be supplied, which is why we speak of combustion with a so-called excess of combustion air.

In modern households (passive houses), the air supply is realized by central ventilation (Fig. 3). This is mainly because the supply of oxygen to the room is no longer possible without direct ventilation (open window / door).



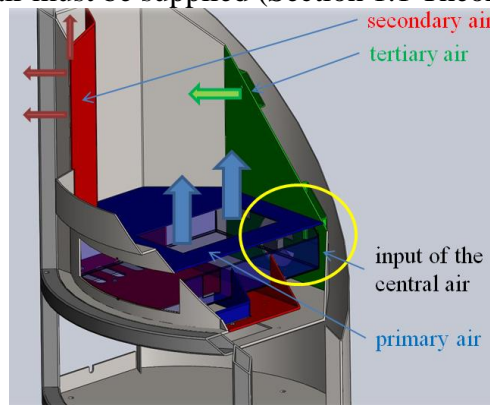
Source: Database of the ABX, spol. s r. o.

Fig. 3: Central input of the air: a) through the chimney; b) central inside air

1.2 Research Objectives

In the hearth (Fig. 4) of the fireplace itself the air must be optimally distributed to supply a sufficient amount of oxygen to the individual combustion phases:

- **primary air** is used at the start of the burning, this air is coming under the grate,
- **secondary air** is used for cleaning glass,
- **tertiary air** is used for better combustion; there exists no ideal combustion, a larger amount of combustion air must be supplied (Section 1.1 Theory).



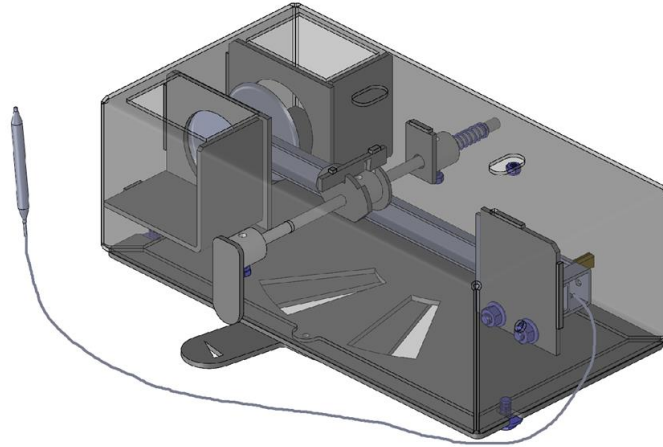
Source: Database of the ABX, spol. s r. o.

Fig. 4: Air in the combustion chamber

Regulation of the input of the air:

- central input air,
- regulation on the door and ashtray,
- regulation on the door only,
- automatic dependence ratio regulation of the primary and secondary air,
- independent innovation of the system of regulation.

State of the art is semi-automatic regulation of the air (Fig. 5).



Source: Database of the ABX, spol. s r. o. (CZ2009823A3)

Fig. 5: Semi-automatic regulation of the air

In the new design, it is very important to do the following:

- change the philosophy of the air damper (dependent versus independent),
- remote controller (for the Arduino system prototype),
- move without human intervention (servo),
- modularization.

1.3 Research Methods

1.3.1 Calculation of the Fuel

When the air is introduced into the combustion chamber, it is necessary to deal with the required fuel dose and its calculation which is governed by formula (1)

$$B_{fl} = \frac{360000 \cdot P_n \cdot t_b}{H_u \cdot \eta} \quad (1)$$

where

B_{fl} is mass of fuel in kg,

H_u is heating value of testing fuel in kJ/kg,

η is efficiency according ČSN EN 13229 or value from official producer in %,

P_n is nominal thermal performance in kW, and

t_b is the shortest delivery time interval of the fuel or period time of the combustion from official producer in hours.

The heating value of the fuel, more precisely the heating value of tree species, is shown in Tab. 1.

Tab. 1: Heating value

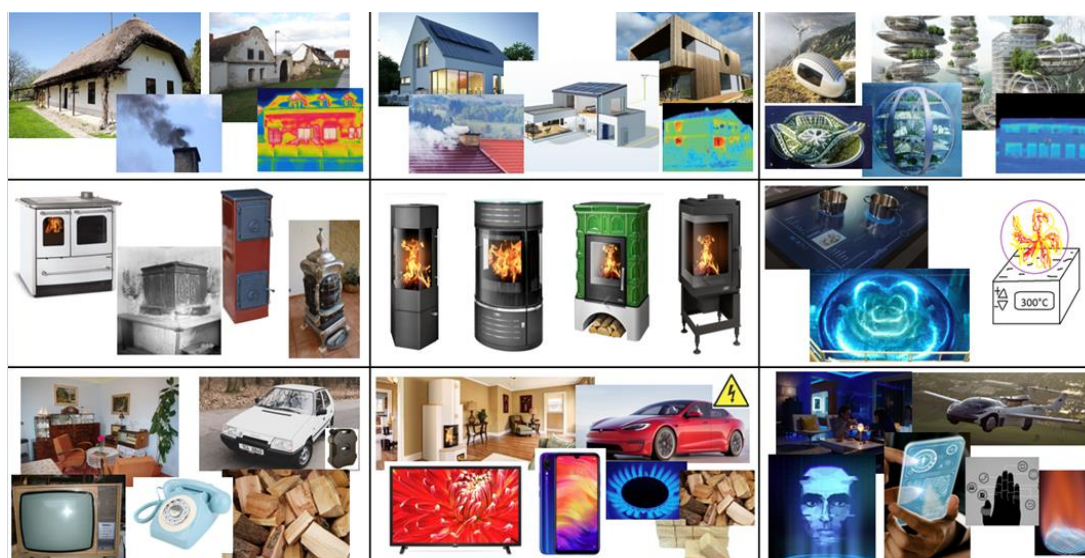
tree species	heating value		
	MJ/kg	MJ/pm	MJ/rm
acacia	12,7	11850,0	8030,0
alder	12,9	8260,0	5550,0
ash	12,7	11010,0	7450,0
beech	12,5	10830,0	7320,0
birch	13,5	10550,0	7100,0
fir	14,0	8040,0	5800,0
hornbeam	12,1	10970,0	7400,0
larch	13,4	9720,0	7040,0
oak	13,2	11050,0	7430,0
pine	13,6	9250,0	6730,0
poplar	12,3	6540,0	4440,0
spruce	13,1	7350,0	5440,0
willow	12,8	8490,0	5740,0

Source: Database of the ABX, spol. s r. o.

When the stove is cold, the controller detects the temperature during temperature detection and favors the primary air intended for wood combustion. As soon as the flue gas temperature rises, the controller gradually throttles the primary air and switches to secondary air for wood combustion. When it is used and the combustion process is resumed, the cycle repeats. The intensity of the combustion is controlled by an air regulator.

1.3.2 9-Screens

A very powerful innovation method is the tool of systematic thinking 9-screens (Fig. 6) because innovators can see connectivity between systems and can prognosticate and predict new direction of innovations.



Source: Database of the ABX, spol. s r. o.

Fig. 6: 9-screens

The pictures in the left column in Fig. 6 are consigned to history, the middle ones show the current situation, and in the right column we can see the possible development in the future.

1.3.3 FEM

The software used for simulations (Fig. 7) is FloXpress for Solidworks Premium 2019 SP 5.0. With this software, the flow of the air passages and what happened inside the equipment were analyzed.

Initial and boundary conditions of FEM model:

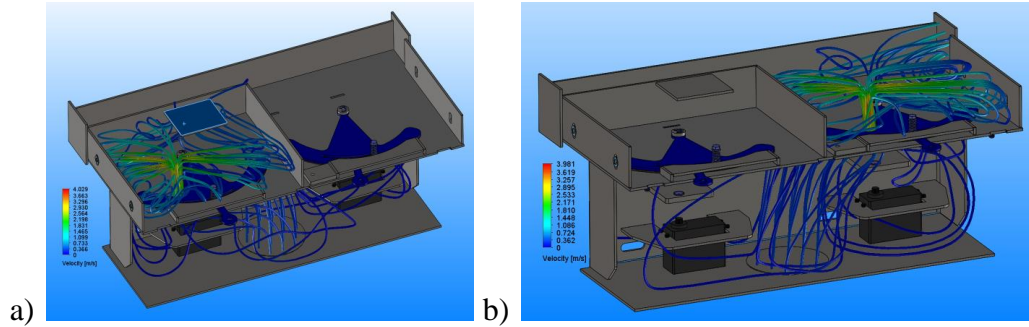
I. input:

- pressure $p_{in} = 101325$ Pa
- temperature $T_{in} = 293.2$ K (Common Temperature Reference Points)

II. output:

- pressure $p_{out} = 101315$ Pa
- temperature $T_{out} = 293.2$ K

Notice: Standard temperature and pressure (STP) are standard sets of conditions for experimental measurements to be established to allow comparisons to be made between different sets of data.



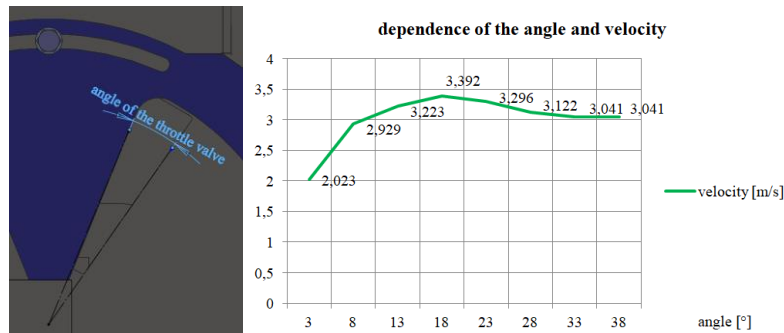
Source: Own

Fig. 7: FEM study of the air: a) primary; b) secondary

According to the outputs from the virtual analysis air passages and upper plate, which divide the air distribution into primary and secondary parts, have been modified.

The virtual analysis has also revealed the velocity of the flowing medium (air) (Fig. 8), which is similar in both the primary and the secondary cases and reaches $v_{max} = 4.029 \text{ m} \cdot \text{s}^{-1}$.

For the primary air, the dependence of the throttle rotation angle and the maximum air flow rate was determined. Dramatic dependence is obvious on the start opening of the throttle valve (from $3^\circ \div 13^\circ$). It is very important information since it has basic effect for combustion.

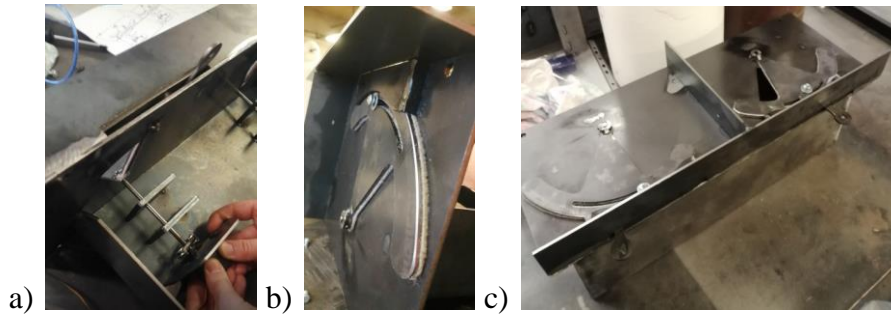


Source: Own

Fig. 8: Dependence of the angle and velocity of the primary air

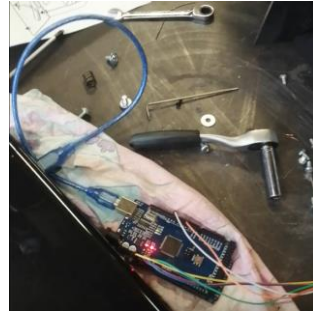
1.3.4 Operational Test

In this case, the virtual analysis cannot be fully trusted. For final resolutions the verification is needed. Operational test is necessary (Fig. 9). Test of the independent electronic air control has focused at the assembly (design for assembly) and soft move of air dampers. Functionality was priority (Fig. 10).



Source: Own

Fig. 9: Operational test: a) Test of assembly; b) Detail view of the throttle; c) Current part



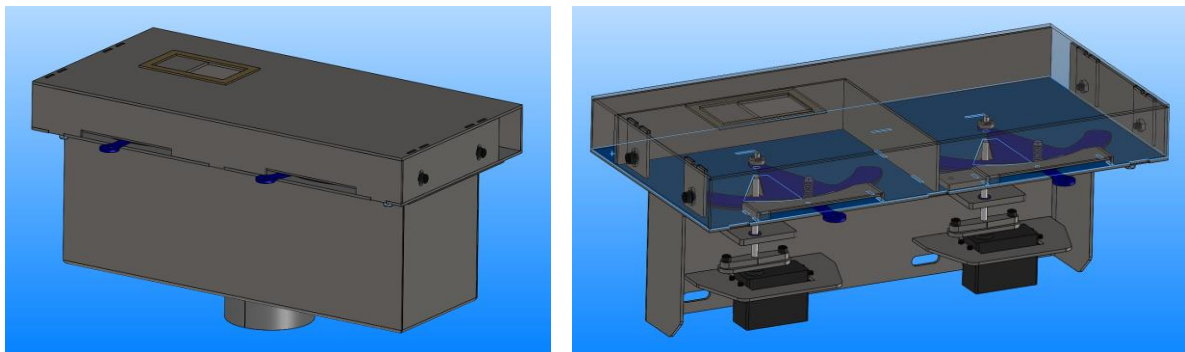
Source: Own

Fig. 10: Operational test; Arduino connectivity

2 Final Design

2.1 3D Model

The assembly of the electronic independent equipment is shown in Fig. 11. 3D software for models is Solidworks 2019 SP 5.0.



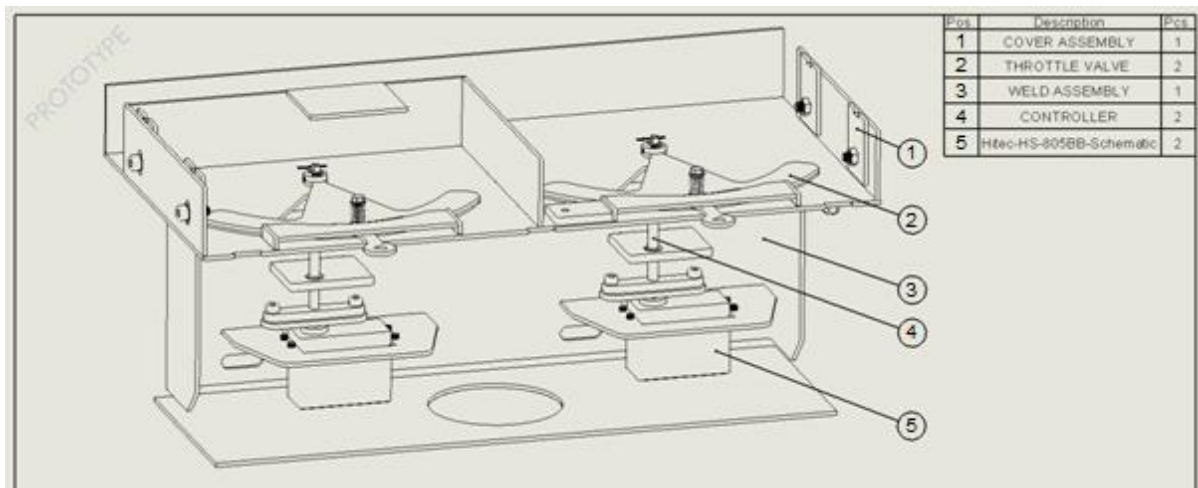
Source: Own

Fig. 11: 3D model

2.2 2D Drawing

The main parts are shown in Fig. 12 as 2D drawing documentation where

- pos. 1 is cover assembly (only few parts are visible),
- pos. 2 is throttle valve (for primary and secondary air is same shape),
- pos. 3 is weld assembly (material is S235J according EN 10025-2), and
- pos. 4 is controller / mechanism assembly (major component is the axis for the adjustment of the angle).

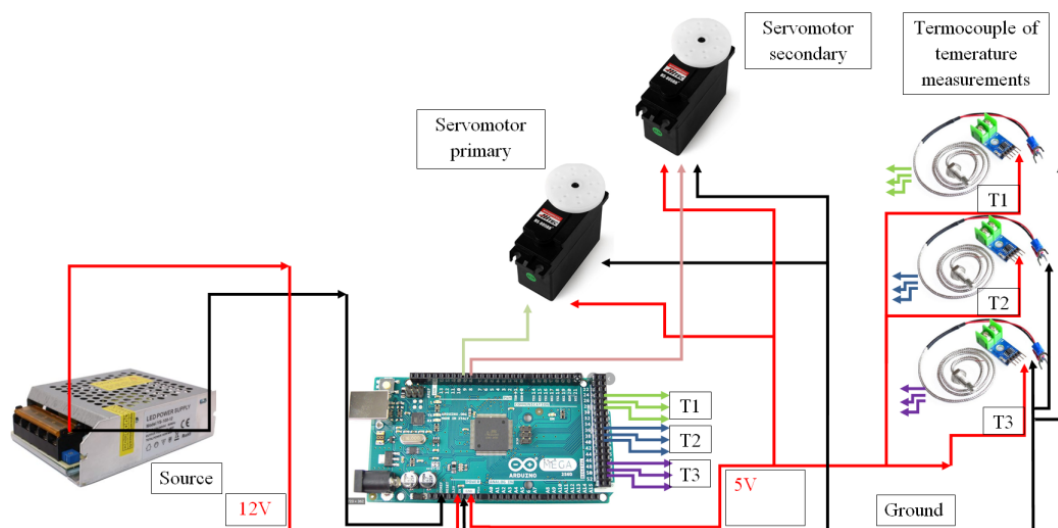


Source: Own

Fig. 12: 2D Drawing with main position

2.3 Electronic System

Arduino (Fig. 13) has been chosen for prototyping. It is hobby equipment, however, a cheap, sufficient and good solution for this phase, which was the reason for implementation.



Source: Database of the ABX, spol. s r. o.

Fig. 13: Schema of the electronic wiring diagram

3 Result and Discussions

The manufacture and installation of electronic air control equipment revealed:

- A minor design imperfection, the controller shaft guide was made (bearings and holes).
- An operational test has shown that it is most likely unnecessary to use a throttle compression spring. The throttle valve pressure uses gravity and makes pressure by the weight of the air damper itself.
- The throttle valve moves in the desired trajectory without scrubbing and squeaking.
- Holes are sufficiently sealed.

The test results also show that the original idea to build an electronic system on a 'hobby' Arduino for the prototype phase was correct. However, **for industrial use it will be necessary to use more sophisticated equipment integrated into the printed circuit board (PCB).**

Conclusion

The main advantage of regulation lies in the independent division of the primary and secondary air and in the purity of combustion.

With normal stoves, it is possible to degrade the purity of flue gases and other measured quantities to a level that does not comply with the EN 13240 standard (or German Din + and Austrian A 15) by incorrectly setting the ratio of primary and secondary air. Adjusting the air according to the test in the laboratory room is almost impossible for an ordinary person heating with normal stoves.

On the contrary, with automatic control the ratio is set automatically.

The regulation works on the principle of sensing the flue gas temperature and then, according to the flue gas temperature, which is sensed by a sensor, the dampers divide the ratio of primary air coming under the grate and secondary air (it is passing through channels and along the glass – supports the purity of wood burning).

- The innovation of setting the air passage of fireplaces has met with success.
- Dependent philosophy was changed to the independent control.
- Move without human intervention (servo) was realized.
- Modularization with 3D model was created, and device was virtually analyzed using the finite element method.
- The equipment was manufactured thanks to FEM analysis where only local minor modifications occurred, and the system was physically tested with acceptable results.

What is important for the future research steps:

- To make whole fireplace stoves with modular independent control of primary and secondary air.
- To perform comprehensive operational testing and further development of the system (research and develop the remote controller).

Acknowledgements

This work was supported by the financial fund of ABX, spol. s r. o., as the integral part of R&D department.

Literature

- [1] SORNEK, K.; FILIPOWICZ, M.; RZEPKA, K.: The development of a thermoelectric power generator dedicated to stove-fireplaces with heat accumulation systems. *Energy Conversion and Management*. 2016, Vol. 125, pp. 185–193. DOI: [10.1016/j.enconman.2016.05.091](https://doi.org/10.1016/j.enconman.2016.05.091)
- [2] GROSS, P. L.; BUCHANAN, N.; SANÉ, S.: Blue skies in the making: Air quality action plans and urban imaginaries in London, Hong Kong, and San Francisco. *Energy Research & Social Science*. 2019, Vol. 48, pp. 85–95. DOI: [10.1016/j.erss.2018.09.019](https://doi.org/10.1016/j.erss.2018.09.019)

INOVACE ELEKTRONICKÉ REGULACE VZDUCHU V KRBOVÝCH KAMNECH

Systém elektronické dusivky slouží k automatizovanému řízení rozvodu vzduchu v krbových kamnech bez zásahu člověka. Je navržen tak, aby splňoval stanovená kritéria, jako je primární a sekundární rozvod vzduchu, šetrnost k životnímu prostředí a snadná výměna a servis funkčních dílů. Klasická krbová kamna lze regulovat pomocí primárního a sekundárního vzduchu, které jsou ovládány manuálně nebo v kombinaci s automatickou klapkou. Běžný uživatel není schopen vyladit poměr primárního a sekundárního vzduchu v poměru, který je vyzkoušený ve státní zkušební laboratoři. Běžný uživatel většinou ani nezná pojmy sekundární a primární vzduch. Je tedy nezbytné systém ovládání vzduchu inovovat.

INNOVATION DER ELEKTRONISCHEN LUFTREGELUNG IN KAMINÖFEN

Das elektronische Luftklappensystem dient zur automatisierten Regelung der Luftverteilung in Kaminöfen ohne menschliches Eingreifen. Es ist so konzipiert, dass es bestimmte Kriterien wie Primär- und Sekundärluftverteilung, Umweltfreundlichkeit und einfachen Austausch und Service von Funktionsteilen erfüllt. Klassische Kaminöfen können mit Hilfe von Primär- und Sekundärluft geregelt werden, die manuell bedient werden, auch während der Verbrennung, oder in Kombination mit einer automatischen Klappe. Der Normalbenutzer ist nicht in der Lage, das Verhältnis von Primär- und Sekundärluft auf das im staatlichen Prüflabor erprobte Verhältnis einstellen. Der Normalbenutzer kennt in der Regel nicht einmal die Begriffe Sekundär- und Primärluft. Es ist notwendig, das System der Luftkontrolle zu erneuern.

INNOWACJA ELEKTRONICZNE USTAWIENIE POWIETRZA DO PIECA KOMINKOWEGO

Elektroniczny system dławika służy do automatycznego sterowania dystrybucją powietrza w kominkach bez ingerencji człowieka. Został zaprojektowany tak, aby spełniał ustalone kryteria, takie jak dystrybucja powietrza pierwotnego i wtórnego, przyjazność dla środowiska oraz łatwa wymiana i serwis części funkcjonalnych. Kominki klasyczne mogą być regulowane za pomocą powietrza pierwotnego i wtórnego, które sterowane są ręcznie podczas spalania lub w połączeniu z przepustnicą automatyczną. Przeciętny użytkownik nie jest w stanie dostroić stosunku powietrza pierwotnego i wtórnego w stosunku, który jest testowany w państwowym laboratorium badawczym. Przeciętny użytkownik zwykle nie zna nawet terminów powietrze wtórne i pierwotne. Konieczna jest innowacja systemu kontroli powietrza.




LIST OF AUTHORS

Name	E-Mail and Page Number of Contribution	
Jan Bělik	jan.belik@vuts.cz	7
Hamid Castillo Martinez	hamid_omar.castillo_martinez@stud.hszg.de	14
Emiliano Lara Romero	emiliano.lara_romero@stud.hszg.de	14
Ricardo Ugalde Tinoco	ricardo.ugalde_tinoco@stud.hszg.de	14
Christian Vogel	c.vogel@hszg.de	14
Daniel Fiß	d.fiss@hszg.de	30
Stefan Kühnel	s.kuehnel@hszg.de	30
Ernest Krzyszkowski	ernestkk1996@gmail.com	30
Stefan Kornhuber	s.kornhuber@hszg.de	30
Josef Hykl	josef.hykl@tul.cz	46

GUIDELINES FOR CONTRIBUTORS

Guidelines for contributors are written in the form of a template which is available as a Word document at http://acc-ern.tul.cz/images/journal/ACC_Journal_Template.docx.

EDITORIAL BOARD

<i>Editor in Chief</i>  Prof. Ing. Pavel Mokrý, Ph.D.	Technical University of Liberec pavel.mokry@tul.cz
<i>Assistant of the Editor in Chief</i>  Prof. Ing. Miroslav Žížka, Ph.D.	Technical University of Liberec miroslav.zizka@tul.cz
<i>Executive Editor</i>  PaedDr. Helena Neumannová, Ph.D.	Technical University of Liberec helena.neumannova@tul.cz phone: +420 734 872 413

Other Members of the Editorial Board

 doc. PaedDr. Hana Andrášová, Ph.D.	University of South Bohemia in České Budějovice andras@pf.jcu.cz
 doc. PhDr. Tomáš Kasper, Ph.D.	Technical University of Liberec tomas.kasper@tul.cz
 Prof. Ing. Jiří Militký, CSc.	Technical University of Liberec jiri.militky@tul.cz
 doc. Ing. Iva Petříková, Ph.D.	Technical University of Liberec iva.petrikova@tul.cz
 doc. Dr. Ing. Miroslav Plevný	University of West Bohemia in Pilsen plevny@fek.zcu.cz
 doc. Ing. Petr Šidlof, Ph.D.	Technical University of Liberec petr.sidlof@tul.cz
 Dr. Eckhard Burkatzki	TU Dresden / IHI Zittau burkatzki@tu-dresden.de
 Prof. Dr.-Ing. Frank Hentschel	Hochschule Zittau / Görlitz f.hentschel@hszg.de
 Prof. Dr. phil. PhDr. (MU Brno) Annette Muschner	Hochschule Zittau / Görlitz a.muschner@hszg.de
 Dr. Piotr Gryszel	Universitet Ekonomiczny we Wrocławiu Wydział Ekonomii Zarządzania i Turystyki piotr.gryszel@ue.wroc.pl
 Prof. UE Dr. hab. Elżbieta Sobczak	Universitet Ekonomiczny we Wrocławiu Wydział Ekonomii Zarządzania i Turystyki elzbieta.sobczak@ue.wroc.pl
 Prof. UE Dr. hab. Grażyna Węgrzyn	Universitet Ekonomiczny we Wrocławiu Wydział Ekonomii Zarządzania i Turystyki grazyna.wegrzyn@ue.wroc.pl

Assistant of the editorial office:

Ing. Dana Nejedlová, Ph.D., Technical University of Liberec, Department of Informatics,
phone: +420 485 352 323, e-mail: dana.nejedlova@tul.cz

Název časopisu (<i>Journal Title</i>)	ACC JOURNAL
Rok/Ročník/Číslo (<i>Year/Volume/Issue</i>)	2022/28/1 (2022/XXVIII/Issue A)
Autor (<i>Author</i>)	kolektiv autorů (<i>composite author</i>)
Vydavatel (<i>Published by</i>)	Technická univerzita v Liberci Studentská 2, Liberec 1, 461 17 IČO 46747885, DIČ CZ 46 747 885
Schváleno rektorem TU v Liberci dne	25. 2. 2022, č. j. RE 6/22
Vyšlo (<i>Published on</i>)	30. 6. 2022
Počet stran (<i>Number of pages</i>)	58
Vydání (<i>Edition</i>)	první (<i>first</i>)
Číslo publikace (<i>Number of publication</i>)	55-006-22
Evidenční číslo periodického tisku (<i>Registry reference number of periodical print</i>)	MK ČR E 18815
Počet výtisků (<i>Number of copies</i>)	60 ks (<i>pieces</i>)
Adresa redakce (<i>Address of the editorial office</i>)	Technická univerzita v Liberci Akademické koordinační středisko v Euroregionu Nisa (ACC) Studentská 2, Liberec 1 461 17, Česká republika Tel. +420 485 352 318, Fax +420 485 352 229 e-mail: acc-journal@tul.cz http://acc-ern.tul.cz
Tiskne (<i>Print</i>)	Vysokoškolský podnik Liberec, spol. s r.o. Studentská 1402/2, Liberec 1 460 01, Česká republika

Upozornění pro čtenáře

Příspěvky v časopise jsou recenzovány a prošly jazykovou redakcí.

Readers' notice

Contributions in the journal have been reviewed and edited.

Předplatné

Objednávky předplatného přijímá redakce. Cena předplatného za rok je 1050,- Kč mimo balné a poštovné. Starší čísla lze objednat do vyčerpání zásob (cena 350,- Kč za kus).

Subscription

Subscription orders must be sent to the editorial office. The price is 40 € a year excluding postage and packaging. It is possible to order older issues only until present supplies are exhausted (8 € an issue).

Časopis ACC JOURNAL vychází třikrát ročně (červen, září, prosinec).

Three issues of ACC JOURNAL are published every year (June, September, December).

Liberec – Zittau/Görlitz – Wrocław/Jelenia Góra

© Technická univerzita v Liberci – 2022

ISSN 1803-9782 (Print)

ISSN 2571-0613 (Online)